Late Paleozoic tectonic evolution of the Paleo-Asian Ocean in the northern Alxa Block (NW China)

Rongsong Tian[1], Guoai Xie[1]*, Wenbin Zhu[1]*, Jin Zhang[2], Shuang Gao[1], Beihang Zhang[2], Heng Zhao[2], Tian Li[1]

1. State Key Laboratory for Mineral Deposits Research, Institute of Continental Geodynamics, School of Earth Sciences and Engineering, Nanjing University, Nanjing, 210093, China; 2. Key Laboratory of Deep–Earth Dynamics of Ministry of Natural Resources, Institute of Geology, Chinese Academy of Geological Sciences, Beijing, 100037, China

Corresponding author, Tel.:+86 138518928465.

E-mail address: xganju@126.com (G. Xie); zwb@nju.edu.cn (W. Zhu)

Key points:

- Early – middle Permian continental volcanic arc was recognized in Nuoergong – Langshan Zone in the northern Alxa Block.
- Permian subduction and crustal thickening processes existed along the southern Central Asian Orogenic Belt (CAOB).
- Transcurrent dextral shear zone developed in the southern CAOB, probably resulting from the lateral extrusion of the thickened crust.

Abstract: The northern Alxa Block occupies a key position in the southern margin of

Central Asian Orogenic Belt (CAOB) and records late Paleozoic subduction and closure processes of the Paleo–Asian Ocean (PAO). However, there are still controversies regarding the timing and location of the final closure of the PAO. This study presents structural deformation data, geochronological and geochemical data for Permian volcanic rocks, as well as detrital zircon provenance analysis of Permian sedimentary rocks along the Nuoergong - Langshan Zone (NLZ) in the northern Alxa Block. During the Carboniferous to middle Permian, the Paleo-Asian Ocean (PAO) lithospheric slab subducts beneath the northern Alxa Block, rendering a continental volcanic arc in the NLZ and also giving rise to extensive folding, thrusting and crustal thickening. Subsequently, a retroarc foreland basin was developed behind the continental volcanic arc, where pyroclastic material with Carboniferous to Permian ages from the volcanic arc and sediments eroded from the Alxa Precambrian basements were deposited (Dahongshan Formation) during middle Permian (Ca. 261 Ma). A large-scale dextral ductile shear deformation in the NLZ resulting from the lateral extrusion of the thickened crust after the continental collision was constrained between 272 Ma and 249 Ma, suggesting a middle Permian tectonic transition from compression to transpression. Combining with published data, we suggest that the final consumption of the PAO occurred in the middle to late Permian, probably along the Qagan Qulu suture zone in the northern Alxa Block.

1. Introduction

45 The Central Asian Orogenic Belt (CAOB) has undergone long–lived evolution
46 from the Neoproterozoic to the Triassic, forming one of the largest and most complex
47 Phanerozoic accretionary orogenic systems on Earth (Fig. 1a) (Şengör et al., 1993,
48 2018; Windley et al., 2007; Xiao et al., 2013, 2015). The southernmost segment of the
49 CAOB extends from the Tianshan and Beishan orogens in NW China to the Xing' an -
50 Mongolian orogen in NE China and preserves the history of late Paleozoic to early
51 Mesozoic closure of the Paleo–Asian Ocean (PAO) by subduction and subsequent
52 continental collision with the Tarim and North China blocks (Han et al., 2011; Jian et
53 al., 2010; Eizenhöfer and Zhao et al., 2018; Xiao et al., 2015). The northern margin of
54 the Alxa Block occupies a key position in the middle segment of the southernmost
55 CAOB (Fig. 1b) and connects the Beishan and Tianshan orogens to the west and the
56 Xing' an - Mongolian orogen to the east.
57 The timing and location of the final closure of the PAO is crucial for our
58 understanding of the tectonic evolution of the CAOB. Considerable progress on the
59 tectonic evolution of the PAO has been made in the western and eastern segment of
60 the CAOB (Jian et al., 2010; Eizenhöfer et al., 2014; Klemd et al., 2015; Zhang et al.,
61 2015a, 2016a; Wang et al., 2018a) and several related tectonic evolution syntheses
62 have recently been published (Han et al., 2011; Xiao et al., 2015, 2018; Eizenhöfer
63 and Zhao et al., 2018). In the central segment of the CAOB, i.e., the northern margin
64 of Alxa Block, extensive mapping, geochemical and geochronological work have
65 been carried out in recent years (Dan et al., 2014a, b, 2015; Shi et al., 2014a, 2016;
66 Hu et al., 2014; Gong et al., 2012, 2016; J. J. Zhang et al., 2015b, 2016b; Song et al.,

2018a). These studies have established the major magmatic events, basement components and sedimentary records in the northern Alxa Block. However, there are still considerable disagreements regarding the time and location of the final closure of the PAO in this area. Some researchers suggested that the Engger Us ophiolite belt (Fig. 1b) represents the suture zone between the Alxa Block and the southern CAOB (Wu and He, 1993; Zheng et al., 2014), whereas others maintained that the Qagan Qulu ophiolite belt is the location of final closure of the PAO (Shi et al., 2014a, b; J. J. Zhang et al., 2015b). These disagreements primarily stem from different interpretations of tectonic settings during the late Carboniferous to Permian in the northern Alxa Block.

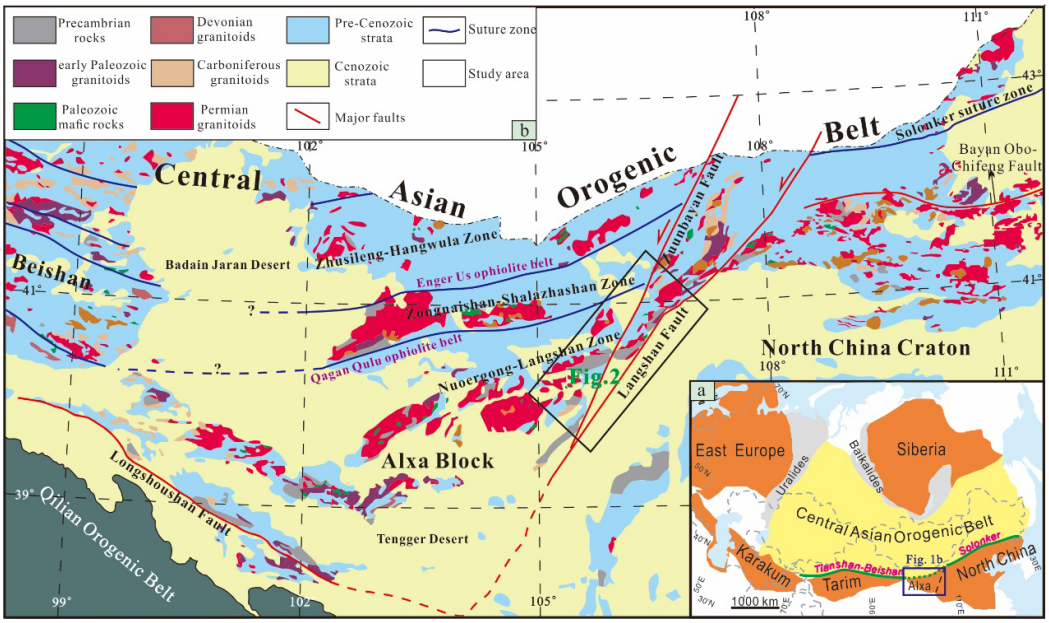

Figure 1. (a) Sketch map of the Central Asian Orogenic Belt showing the location of the Alxa Block. Modified from Xiao et al. (2015); (b) Schematic geological map of the Alxa Block and its adjacent areas, showing the distribution of magmatic rocks and major tectonic boundaries (Modified after Zhang et al. 2015b; Tian et al. 2019).

The timing of the final consumption of the PAO has also been disputed. Several authors suggested an early Permian extension related to a mantle plume (Dan et al., 2014b, 2015) or continental rifting (Zhang et al., 2012; Shi et al., 2018) in the

northern Alxa Block, implying that the PAO has closed before the early Permian. However, many researchers proposed that there is a Carboniferous to middle Permian continental arc setting in this area (Feng et al., 2013; Peng et al., 2013; Yang et al., 2014; Liu et al., 2017a; Song et al., 2018a, b) and argued that the PAO was not consumed until the early to middle Permian. This controversy is mainly due to non-unique interpretations of isotopic and geochemical analyses of the Carboniferous to early Permian plutonic rocks.

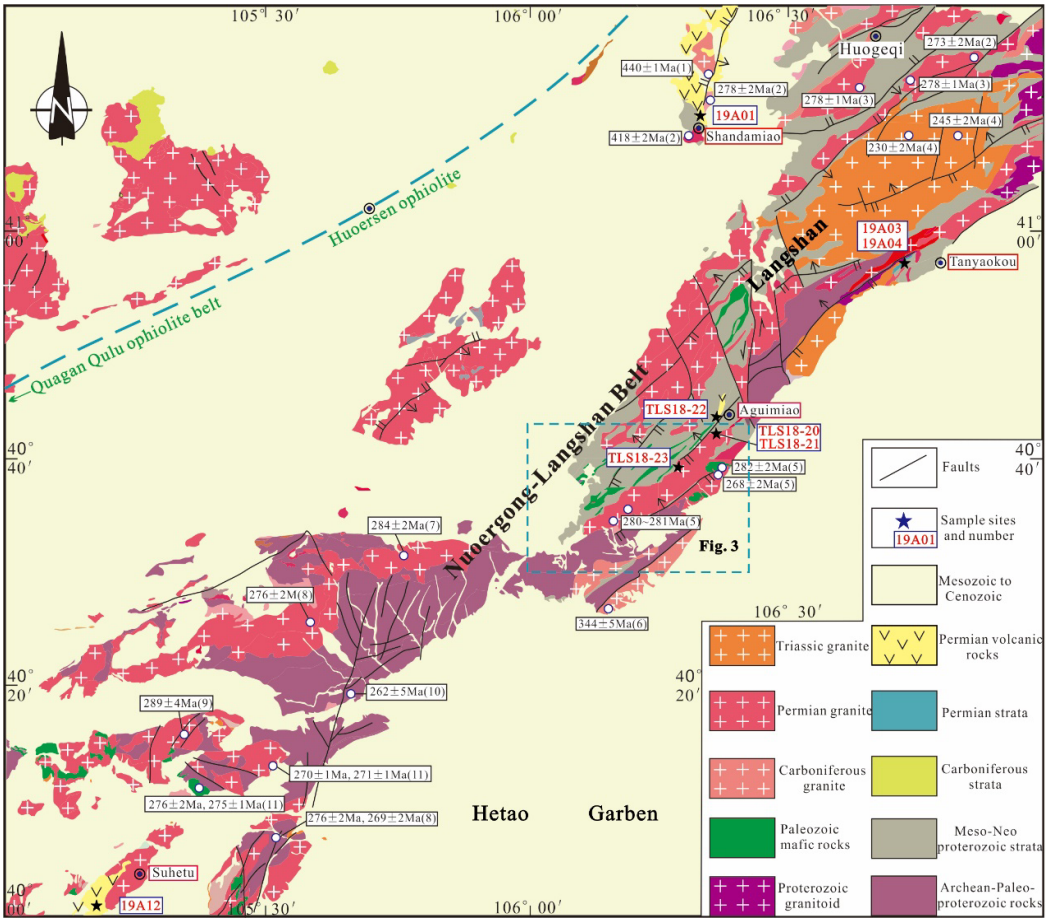

Figure 2. Geological map of the Langshan region showing the distribution of major lithostratigraphic units and sampling locations (modified after 1:200,000 geological maps from the Bureau of Geology and Mineral Resources of Inner Mongolia Autonomous Region (1991). References of geochronological data are listed in Appendix Table S3.

In this paper, we combine structural analysis, zircon U – Pb ages and

geochemistry of Permian volcanic rocks, as well as detrital zircon provenance analysis of Permian strata, to interpret the late Paleozoic tectonic setting in the northern Alxa Block. Our data provide important constraints on the timing and nature of structural and magmatic events in the northern Alxa Block and contribute to establishing a more comprehensive model for the final evolution of the PAO in the southern CAOB.

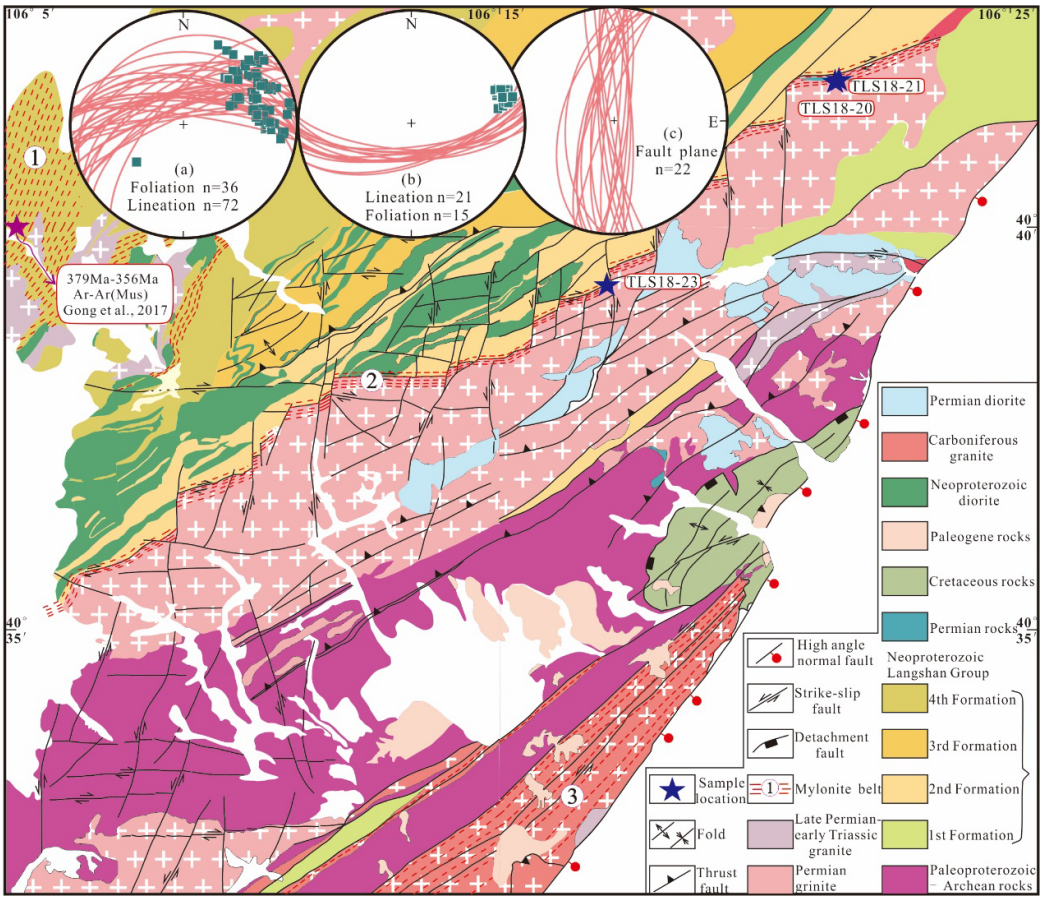

Figure 3. Detailed geological map in the study area showing major structural elements. Stereographic projections show (a) stretching lineations and foliations in granitic mylonites and felsic mylonites in the central and southwestern region, (b) stretching lineations (squares) and foliations in granitic mylonites in the northeastern region, and (c) nearly north–south trending fault planes (lower hemisphere, equal area).

2. Regional Tectonics

111 The Alxa Block is located in a key place that bridges the CAOB to the north,
112 the Tarim Craton to the west and North China Craton to the east (Fig. 1a, b). The Alxa
113 Block is separated by the NE–SW trending Langshan Fault from NCC and by the
114 Longshoushan Fault from the early Paleozoic North Qilian Orogenic Belt. The
115 western and southern parts of the Alxa Block are covered by Cenozoic sediments of
116 the Badain Jaran Desert and Tengger Desert, respectively (Fig. 1b).

117 The Archean–Paleoproterozoic basement rocks occur in the Alxa Block and
118 record similar magmatic–metamorphic events with those in the NCC, suggesting that
119 the Alxa Block is the westernmost part of NCC, either as a part of the Khondalite Belt
120 or the Yinshan Block (J. X. Zhang et al., 2013b; Gong et al., 2016). However, the
121 discovery of Neoproterozoic S–type granite in the Alxa Block and the comparable
122 early Paleozoic detrital zircon age spectra to the South China Craton suggest that the
123 Alxa Block had probably separated from the NCC before the Neoproterozoic (Dan et
124 al., 2014a; J. Zhang et al., 2015c). Despite this controversy, it generally accepted that
125 the northern margins of the Alxa and North China have both experienced tectonic and
126 magmatic events related to the evolution of the PAO and subsequent intracontinental
127 deformation (Zhang et al., 2009a, b; Feng et al., 2013; Wang and Wan. 2014; Liu et al.,
128 2016a).

129 In the northern Alxa Block, two major faults, i.e., the Engger Us Fault and the
130 Quagan Qulu Fault, divide the block into, from north to south, the Zhusileng –
131 Hangwula, Zongnaishan – Shalazhashan and Nuoergong – Langshan zones (Fig. 1b).
132 The Zhusileng – Hangwula Zone (ZHZ) is thought to be the middle part of the

133 southernmost CAOB that extends eastward into Mongolia and is covered by the
134 Badain Jaran Desert to the west. Neoproterozoic metasedimentary rocks are
135 sporadically exposed, including marble, quartzite, sandstone, and phyllite (BGMRNM,
136 1991). Minor granitic gneisses with U–Pb ages of 916Ma and 905Ma were also
137 reported in this zone (Wang et al., 2001; Zhou et al., 2013), indicating a
138 microcontinent with Precambrian basement. During the early Paleozoic, this zone was
139 devoid of volcanic sediments but received a succession of clastic sediments, implying
140 a passive continental margin (Wu and He. 1993). By contrast, late Paleozoic
141 sedimentary sequences are widely distributed in this area and dominantly consist of
142 deep-sea flysh associated with volcanic sediments (BGMRNM, 1991). Late
143 Ordovician (453Ma) and Carboniferous to Permian granitoids (313~277Ma) have
144 recently been identified in this zone (Han et al., 2010; Xu et al., 2013).

145 The Zongnaishan–Shalazhashan Zone (ZSZ) is bounded by the Enger Us Fault
146 to the north and the Qagan Qulu Fault to the south and is covered by Cenozoic
147 sediments to the west and sinistrally displaced by the NE–SW trending Zuunbayan
148 Fault and Langshan Fault (Fig. 1b). Its eastern extension is unclear. Permian
149 granitoids and gabbros and early Triassic granitoids make up the main body of the
150 Zongnaishan and Shalazhashan (W. Zhang et al., 2013a; Shi et al., 2014a, b). Minor
151 late Carboniferous granitoids also occur in this region (Yang et al., 2014). The
152 Amushan Formation is the dominant Paleozoic sedimentary units in this area and is
153 mainly composed of volcanic rocks, neritic carbonate rocks and clastic sediments,
154 which has recently been explained to have been deposited during the Carboniferous

to early Permian (Yin et al., 2016). Some Precambrian high-grade metamorphic rocks are exposed in the Zongnaishan area, which yielded zircon U–Pb ages of ca 1.4 Ga (Shi et al., 2016). However, the ca.1.4Ga magmatic events are rare in the Alxa Block and the NCC. Moreover, available geochronological data do not support the existence of Archean–Paleoproterozoic basement in the ZSZ. Some authors hence suggested that the ZSZ has an affinity with the microcontinental blocks in the CAOB (Zhang et al., 2015b; Shi et al., 2016).

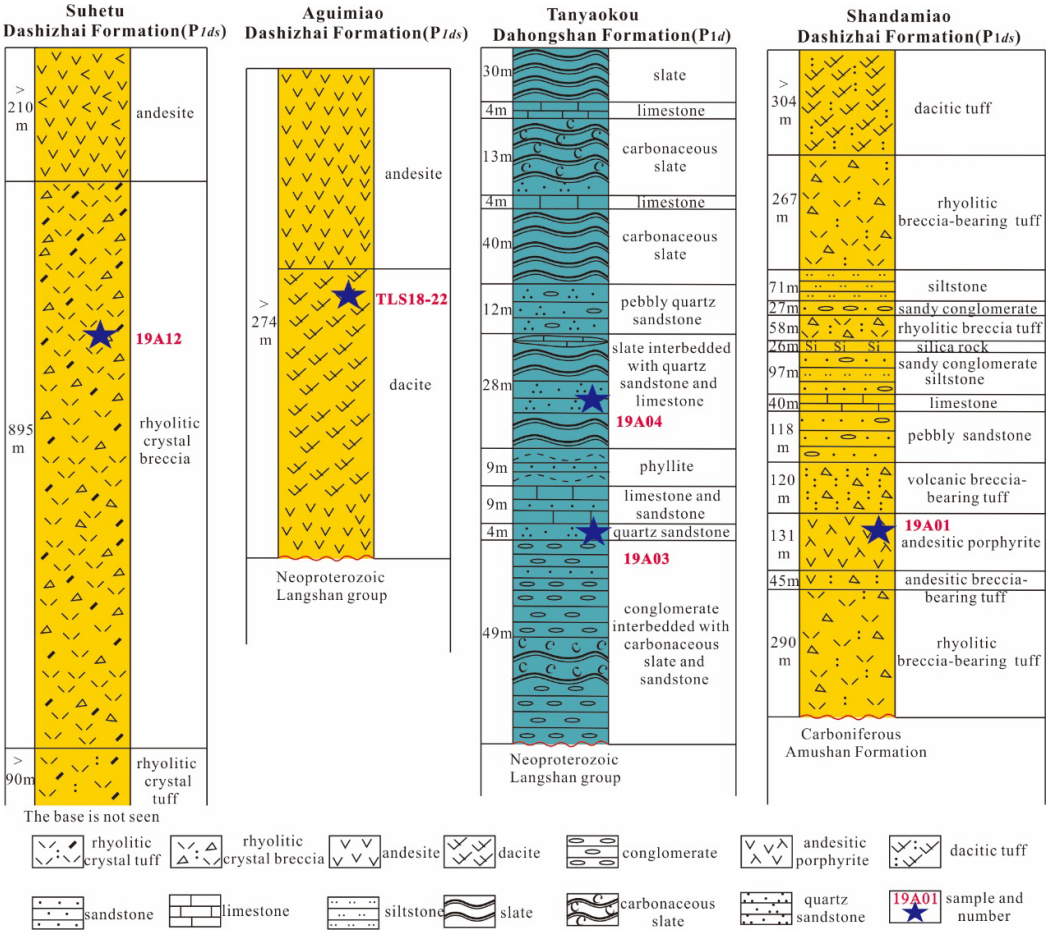

Figure 4. Stratigraphic column of Permian volcano–sedimentary rocks from the Langshan region. Modified from BGMRNM (1991). Positions of the samples in this study are indicated.

The Nuoergong – Langshan Zone (NLZ) is located to the south of the Quagan Qulu ophiolite belt (Fig. 1b). In this zone, Precambrian metamorphic basement rocks

are widely exposed along the Bayanwulashan, Longshoushan, Beidashan, and Langshan (J.X. Zhang et al., 2013b; Gong et al., 2016; Dan et al., 2012). Neoproterozoic to early Paleozoic magmatic rocks are sporadical (Dan et al., 2014a; Liu et al., 2016b). Instead, large volumes of Carboniferous to Permian igneous rocks, including granites, diorites, mafic–ultramafic rocks and intermediate–acid volcanic rocks are exposed in this zone. In the Langshan region, Carboniferous to Permian granite suffered extensive ductile shear deformation. Besides, a Triassic alkaline–rich intrusion belt also occurs in the NLZ (Ren et al., 2005).

3. Geology of the Langshan zone

The Langshan zone, trending northeast for nearly 160 km along the western margin of the Hetao Garben, is part of the NLZ in the northeastern Alxa Block (Fig. 1b). Precambrian rocks in this belt include late Archean to Paleoproterozoic metamorphic rocks (the Wulashan Group and the Diebusige Group) and Neoproterozoic meta–sedimentary rocks (the Langshan Group) (Fig. 2). The Neoproterozoic Langshan Group dominantly consists of crystalline limestone, quartz sandstone, mica–quartz schist and carbonaceous schist, quartzite. Paleozoic sedimentary record is rare in this belt, and only Permian volcanic rocks and minor clastic sediments are sporadically exposed in the Shandamiao, Tanyaokou, Aguimiao and Suhetu areas (Fig. 2). In the Shandamiao area, the Permian strata are dominantly composed of rhyolitic tuff, andesitic porphyrite, dacitic tuff, and minor sandstone and

siltstone. In the Aguimiao area, the volcanic rocks, mainly andesite and dacite in composition, are unconformably overlying the Langshan Group (Fig. 4). The rhyolite with rhyotaxitic structure (Fig. 7f) and andesite distribute in the Suhetu area, which was intruded by Triassic alkaline–rich rocks. The volcaniclastic rocks along the Langshan belt were not formally named by the previous 1:200,000 mapping. Recently, these rocks were mapped as the Dashizhai Formation and attributed to early and middle Permian (Guo et al., 2017). The Dahongshan Formation in the Tanyaokou area is mainly conglomerate, carbonaceous slate, quartz sandstone, and limestone, which unconformably overlies on the Neoproterozoic Langshan Group (Fig. 7a, b). This formation was considered to be formed in the early Permian based on stratigraphic correlation (BGMRNHAR, 1982) but chronological data are lacking. Despite its significance in evaluating the tectonic setting, the Permian strata in the Langshan belt have hitherto been poorly investigated.

In the late Paleozoic, the Langshan belt experienced extensive thermo–tectonic and deformation events in response to the southward subduction and closure of the Paleo–Asian Ocean plate along the northern margin of the Alxa Block. Large volume igneous, including granitoids, diorite, basalt, andesite and minor mafic to ultra–mafic rocks were emplaced during this period (Feng et al., 2013; Peng et al., 2013; Dan et al., 2014b; J.J Zhang et al., 2016b). A series of NE–SW thrust faults with SE or NW dips widely developed in the Langshan belt (Fig. 2). Widespread folds and thrusts deformation are also observed in this area. The crystalline limestone, sandstone, and quartzite in the Neoproterozoic Langshan group suffered intense compression to form

211 overturned isoclinal folds (Fig.5b, c, d). Their hinge lines are subhorizontal to slightly
212 dipping and strike to the northeast or southwest (Fig. 5b). The Paleoproterozoic
213 Diebusige Group and the Neoproterozoic Langshan Group are intruded by felsic veins.
214 These veins intruded roughly along the foliation and have also been folded (Fig. 5e, f),
215 indicating these folds developed after the intrusion of felsic veins. In contrast, some
216 felsic veins invaded the core of folds but were not folded (Fig. 5g), suggesting

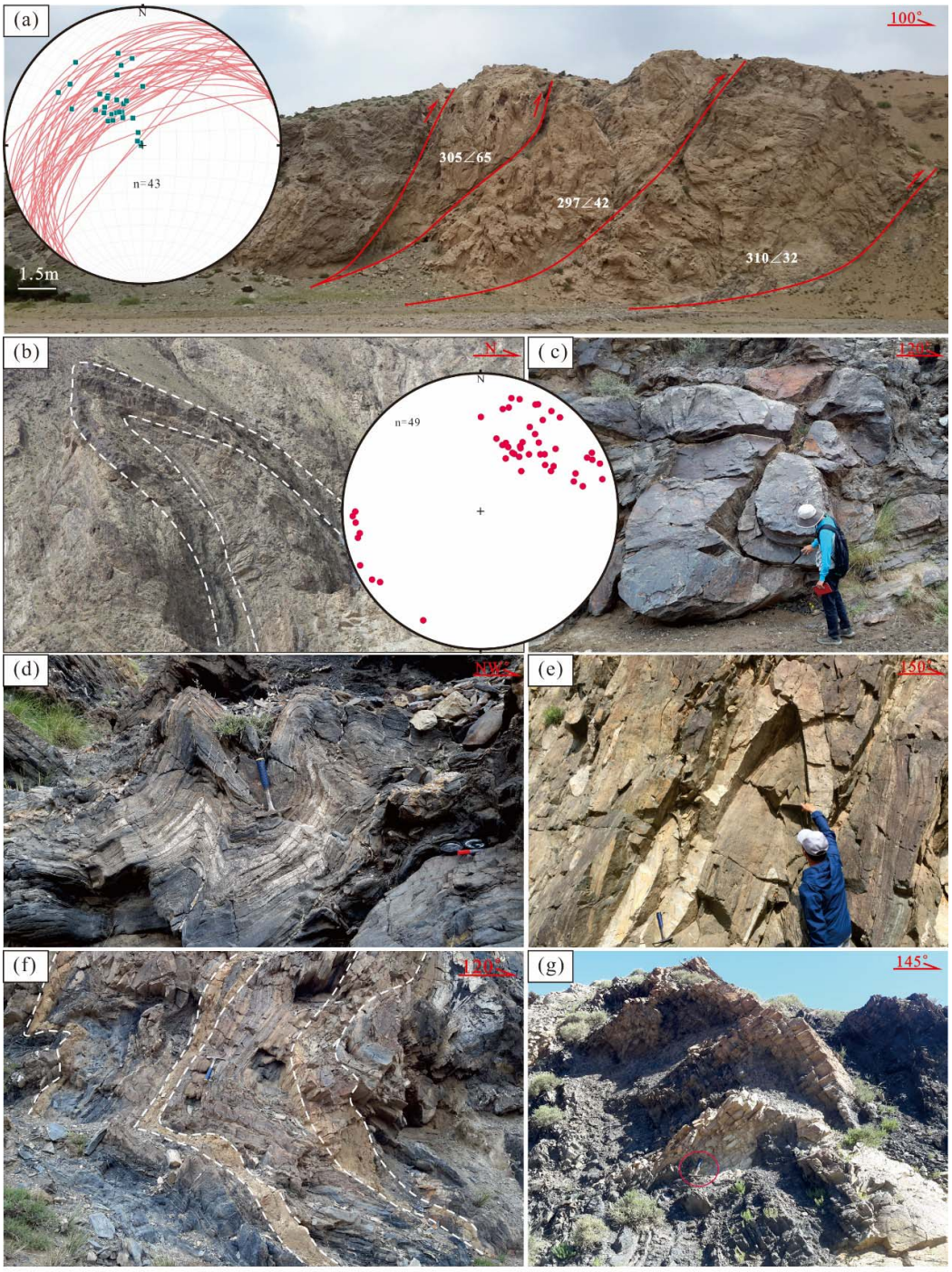

Figure 5. (a) Thrust faults in Permian granite. The great circles in the stereographic projection are fault planes, green spots are slickenlines of the fault planes. (b) Isoclinal overturned fold of crystalline limestone in the Langshan Group; the red spots in the stereographic projection indicate fold hinges. (c) folded thick-bedded quartzite in the Langshan Group. (d) M–type fold in the Langshan Group. (e) Felsic veins intruding the Diebusige Group were also folded (f) Felsic veins intruding the Langshan Group were also folded. (g) Felsic veins intrude the fold core.

intrusion after deformation. Large-scale thrusts and nappes were documented in

225 Permian granitic plutons (Fig. 5a). The fault planes strike NE–SW and dip to NW,

226 pointing to a southeastward thrusting (Fig. 5a).

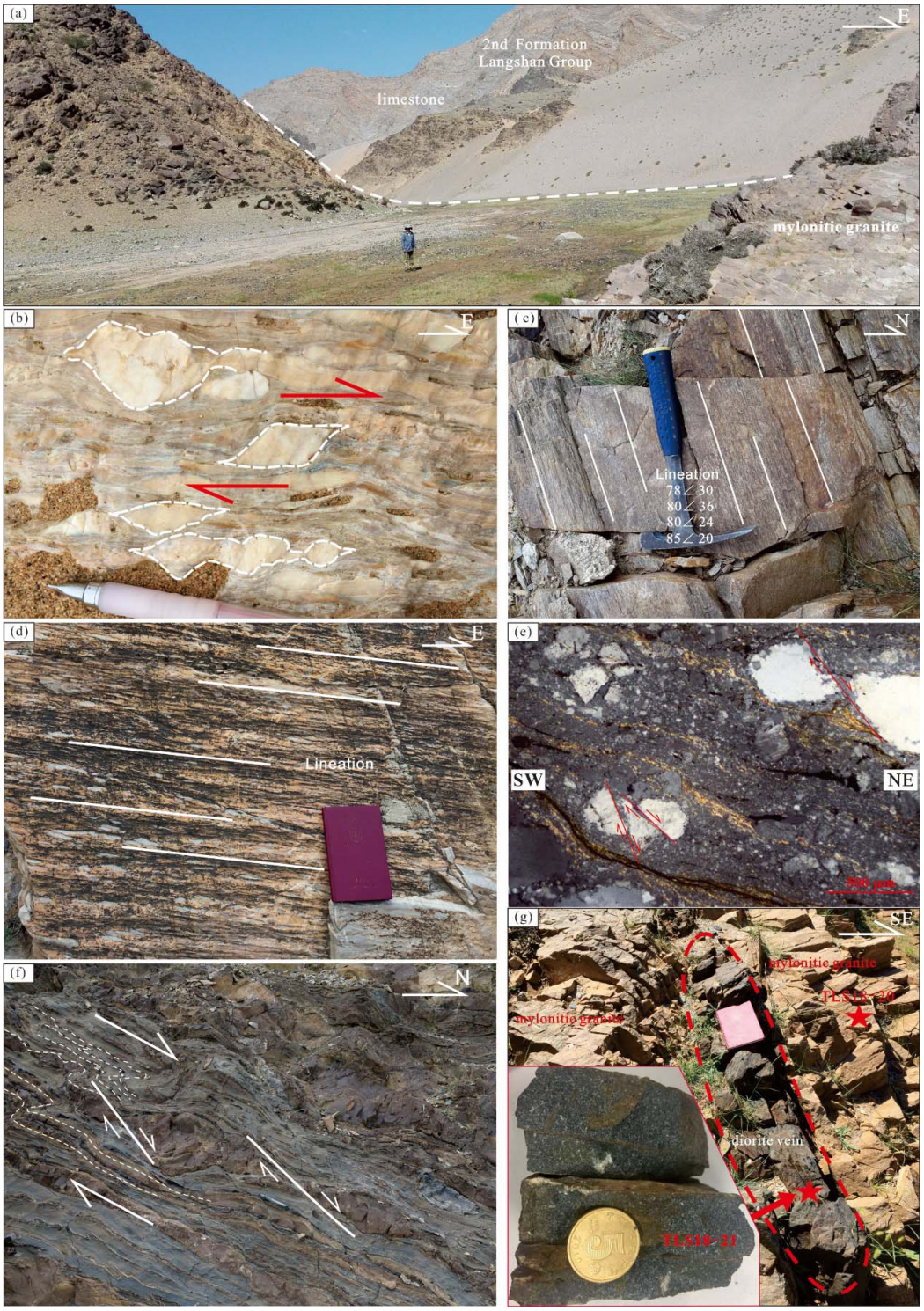

227

228 Figure 6. (a) Dextral ductile strike–slip shear between the Neoproterozoic Langshan Group and the Permian

229 granite pluton. (b) σ–type asymmetric calcite porphyroclast in the Langshan Group, indicating dextral shearing. (c)

mylonitized granite. (d) mylonitized limestone in the Langshan Group. (e) Photomicrographs of granitic mylonite in cross–polarized light suggest dextral strike–slip shear sense. (f) Deformation of nodular chert and crystalline limestone in the Langshan Group, indicating dextral shearing. (g) An undeformed diorite vein intruded the granitic mylonite.

Strike–slip shear is also widely distributed in the Langshan belt. There are three mylonite belts in the southwestern Langshan belt (Fig. 3). The quartzite and muscovite quartz schist from the Neoproterozoic Langshan Group suffered extensive sinistral ductile shearing. Gong et al. (2017) obtained ~379 Ma and ~356 Ma $^{40}Ar/^{39}Ar$ ages from felsic mylonites, indicting deformation in the Late Devonian. Besides, the NE–trending sinistral ductile shearing along the Langshan – Bayanwula Shan in the southeastern part of the study area was interpreted as the result of the collisional between the Yangtze and North China Blocks during the Triassic (J. Zhang et al., 2013c).

In our field mapping, we discovered, for the first time, a ductile dextral shear zone, which developed along the boundary between the Neoproterozoic Langshan Group and the Permian granite pluton (Fig. 3 and Fig. 6a). The dextral shear zone extends continuously for ~30 km in our mapping area with a maximum width of ~1 km and is covered by Quaternary sediments further to the southwest (Fig. 3). The mylonitic foliations in the shear zone generally strike NEE–SWW and dip to the north or south at steep to nearly vertical angles (Fig. 3a and b). In the study area, the mylonitic foliations were partly dislocated by a series of nearly north–south left–lateral strike–slip faults (Fig. 3), which induced a clockwise rotation and thus formed nearly east–west foliations (Fig. 3a, b). The stretching lineations in the shear zone are defined by the preferred alignment of mica, feldspar, and quartz ribbon. Most

stretching lineations are subhorizontal in the shear zone (Fig. 3a, b and Fig. 6c). Based on the field investigation and microscopic observation, kinematic fabrics are widely distributed in the granitic mylonite belt, including σ–type asymmetric quartz augens, fish–like structures and quartz recrystallized tails (Fig. 6e). Several types of microstructures can also be observed, such as undulatory extinction and deformation bands in deformed quartz grains, dynamic recrystallization, and core–mantle structures (Fig. 6e). The Neoproterozoic Langshan Group has also undergone extensive deformation near the boundary. Large volumes of crystalline limestone in this Group have been mylonitized (Fig. 6d). Several kinematic indicators developed, including boundinage of chert and σ–type asymmetric calcite porphyroclast (Fig. 6b, f). All these deformation characteristics indicate a dextral sense of shearing.

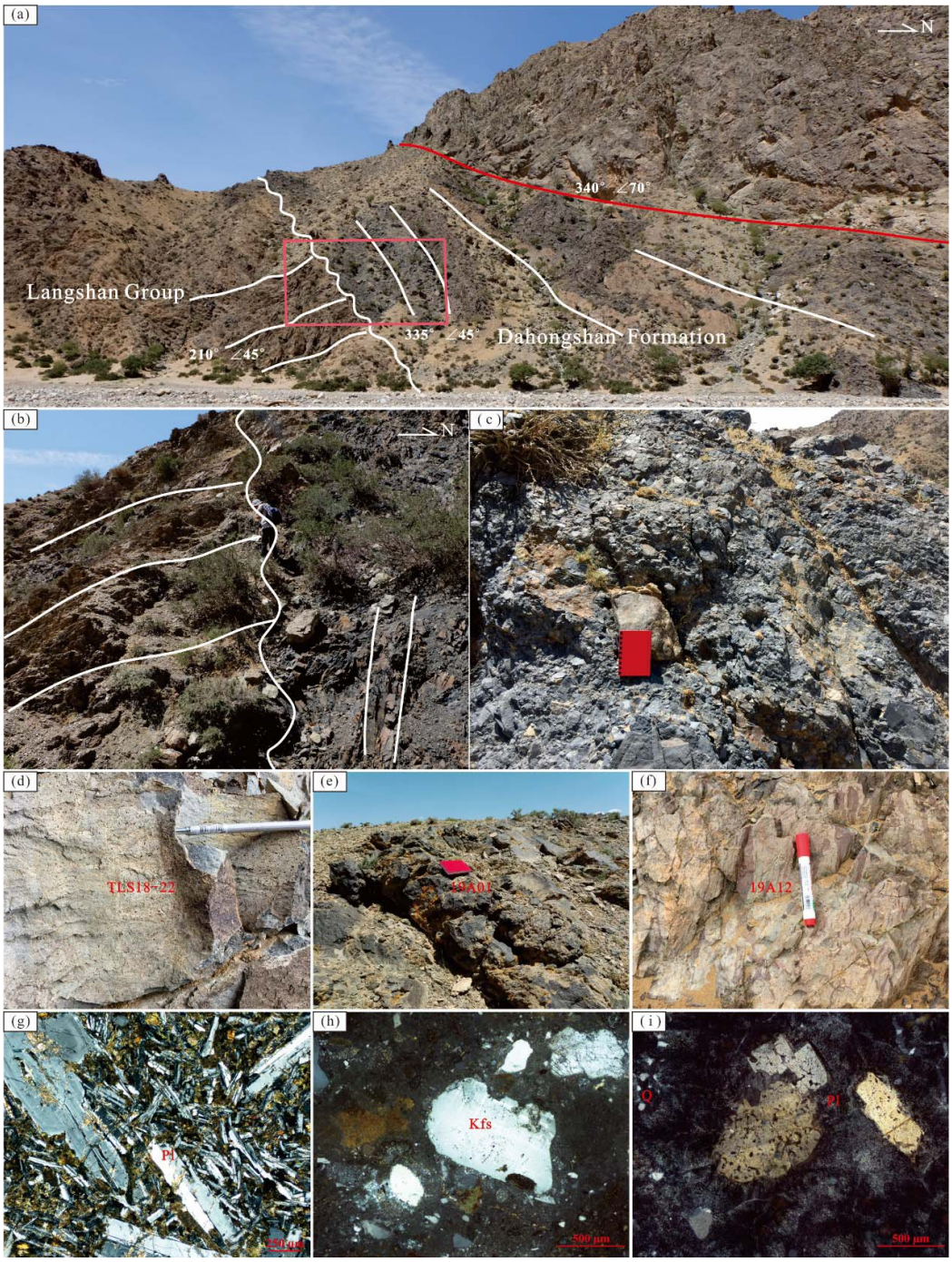

Figure 7. Field and photomicrographs of Permian clastic sediments and volcanic rocks. (a) and (b) The angular unconformity between the Permian Dahongshan Formation and the Neoproterozoic Langshan Group; (c) Conglomerate from the Permian Dahongshan Formation; (d) and (g) Field and photomicrographs of andesite from the Aguimiao area; (e) and (h) Field and photomicrographs of dacite from the Shandamiao area; (f) and (i) Field and photomicrographs of rhyolite from the Suhetu area.

4. Sample description

To evaluate the age and tectonic setting for magmatism, sedimentation and ductile deformation, different types of samples were collected and analyzed from the Langshan belt in this study. The sampling locations are shown in Fig. 2, 3 and 4. The GPS coordinates of the samples are presented in Appendix Table S1. Three volcanic samples (19A01, 19A12 and TLS18–22) were collected for zircon U - Pb dating, as well as major and trace element analyses. Sample 19A01 is a dacite collected from the Shandamiao area, which contains phenocrysts of euhedral–subhedral potassium feldspar (25–30 vol.%), plagioclase (10–15 vol.%) and xenomorphic quartz (10–15 vol.%). The groundmass shows cryptocrystalline texture that is mainly composed of plagioclase, quartz and accessory minerals, such as zircon and apatite. The sample (19A12) was collected from the Suhetu area and is rhyolite in composition, containing ~20 vol.% plagioclase phenocrysts and ~10 vol.% quartz phenocrysts. The hyalopilitic texture groundmass is composed of plagioclase microlites and volcanic glass. Sample TLS18–22 is light-green andesite collected from the Aguimiao area, which mainly consists of long prismatic plagioclase with slight alteration (60 vol.%) and hornblende and minor pyroxene. Two quartz sandstone samples (19A03 and 19A04) from the Dahongshan Formation in the Tanyaokou areas were also collected for detrital zircon U–Pb dating. Moreover, two granitic mylonites (TLS18–20 and TLS18–23) in the shear zone and an intruding undeformed diorite vein (TLS18–21) were also collected for zircon U – Pb dating (Fig. 6g).

5. Analytical results

Analytical methods are presented as supplementary material in Tables S1. Zircon U–Pb dating and whole–rock major and trace element compositions of volcanic rocks are available in supporting information Tables S1and S2, respectively. In this study, $^{207}Pb/^{206}Pb$ ages are adopted for zircons older than 1Ga, while $^{206}Pb/^{238}U$ ages are used for zircon younger than 1Ga.

5.1. Zircon U–Pb dating

Zircon grains from sample 19A01 (dacite) are mostly euhedral, with a length of 50~200um. They commonly show oscillatory zoning in CL images and have Th/U ratios between 0.19 and 0.90, indicating a magmatic origin. Zircon U–Pb dating yielded a weighted mean $^{206}Pb/^{238}U$ age of 263 ± 3 Ma (MSWD = 0.18, n = 5; Fig. 8a). This is consistent with the U–Pb ages recently reported from intermediate–basic volcanic rocks north to the sample site (Guo et al., 2017). Twenty-one analyses yielded older ages clustered at 442±2Ma (Fig. 8a), which are interpreted as captured zircon ages. This is consistent with the fact that the underlying rocks of Permian volcanic rocks are Silurian diorites (Wang et al., 2015).

Sample TLS18–22 (andesite) and 19A12 (rhyolite) were collected from the Aguimiao and Suhetu areas in the central and southwestern Langshan belt, respectively. Zircons from these two samples are euhedral and display clear oscillatory growth zoning in CL images. Twenty-seven zircon grains from the andesite (TLS18–22) are analyzed, yielding a weighted mean $^{206}Pb/^{238}U$ age of 270 ± 3 Ma

(MSWD=0.07; Fig. 8c), whereas 22 analyses for the rhyolite (19A12) give a weighted mean age of 273 ±2 Ma (MSWD=0.33; Fig. 8b). These ages are interpreted as the crystallization age of the andesite and rhyolite. Besides, zircon xenocrysts with concordant age of 2538 Ma and 987 Ma are also obtained from the rhyolite (TableS1).

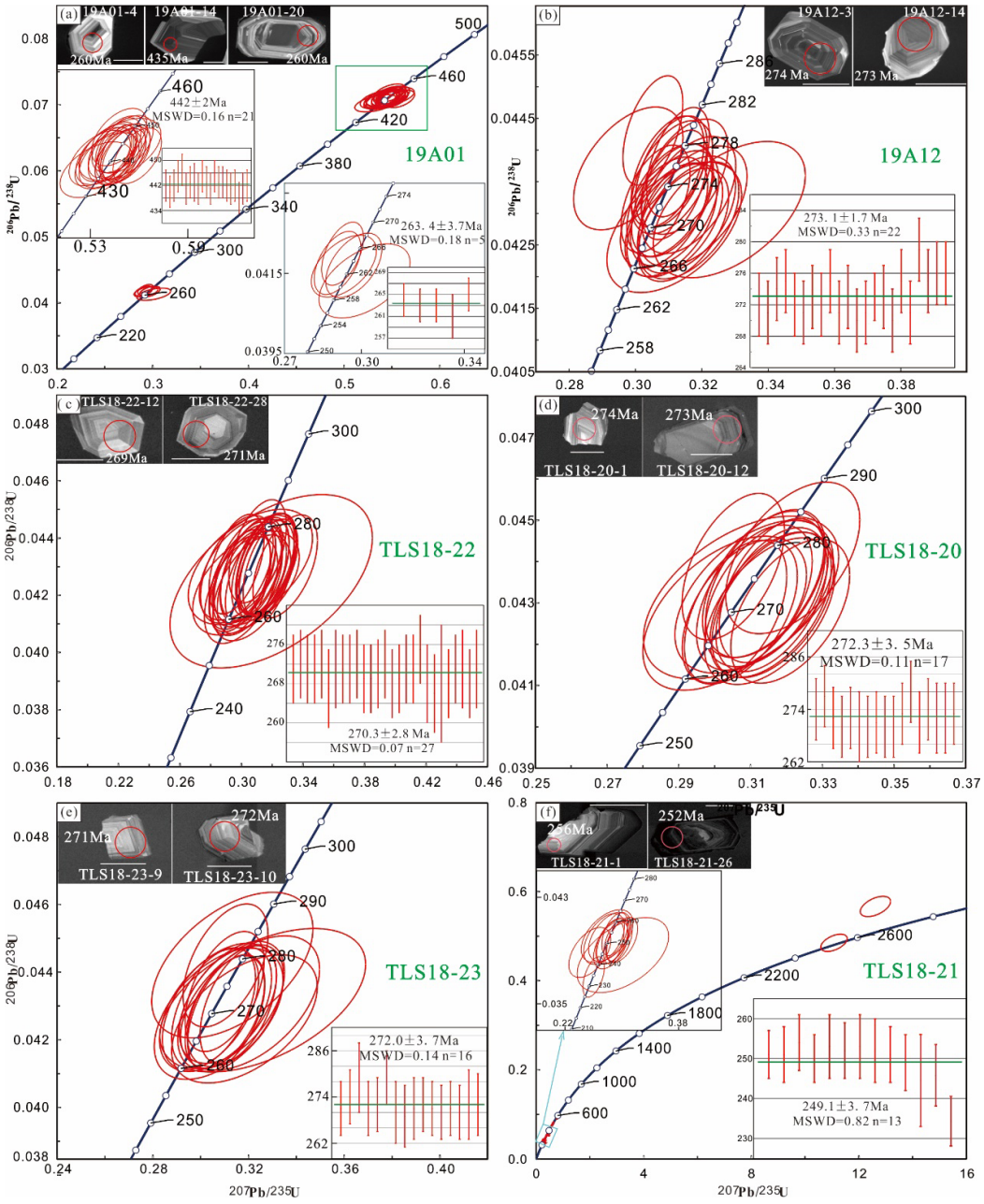

Figure 8. Zircon U–Pb concordia diagrams and histograms for the volcanic rocks and plutons in the Langshan area. (a) Dacite; (b) rhyolite; (c) andesite; (d) and (e) mylonitized granites; (f) undeformed diorite vein

Two granitic mylonite samples (TLS18–20 and TLS18–23) from the dextral shear zone yielded identical zircon U–Pb ages of 272±3.5 Ma and 272±4 3.7 Ma (Fig. 8d, e). Thirteen out of 35 analyzed zircons from the intruding undeformed diorite vein (TLS18–21) form a tight cluster, with a weighted mean $^{206}Pb/^{238}U$ age of 249±4 Ma (MSWD=0.82), which is interpreted as the crystallization age of the undeformed diorite vein. Other analyses mainly yielded two groups of ages, with weighted $^{206}Pb/^{238}U$ ages of 281Ma (MSWD=1.4, n = 7) and 330Ma (MSWD=1.9, n = 6) respectively, which are interpreted as ages of xenocrysts; indeed, early Carboniferous (ca. 330Ma) and early Permian (ca. 280Ma) magmatic rocks have been widely documented in the eastern Alxa Block (Shi et al., 2012; J.J Zhang et al., 2016b; Dan et al., 2016; Zheng et al., 2019b). The remaining two analyses (spots 13 and 14) show much older ages around 2.5 Ga, which are considered as the captured zircons from the crystalline basement (Fig. 8f). These data thus contain the time of the dextral ductile shear deformation between 272 Ma and 249 Ma.

Two sandstone samples (19A03 and 19A04) from the Dahongshan Formation in the Tanyaokou area are used for detrital zircon U-Pb dating. Most zircon grains are euhedral to subrounded, and a few are rounded in shape. Most of the zircon grains exhibit oscillatory zoning with Th/U ratios of 0.11 – 2.79. The ages from sample 19A03 mainly range from 259 Ma to 2484 Ma and cluster around four prominent age peaks at ca. 261 Ma, 289 Ma, 305 Ma, and 1352 Ma, respectively (Fig. 9b). The ages from sample 19A04 mainly range from 272Ma to 3462 Ma, with two main age peaks (318 Ma and 1947 Ma, respectively) and several secondary age peaks (273 Ma, 2388

Ma, and 2509 Ma; Fig. 9d). The youngest detrital zircon age peaks from the two samples constrain the maximum depositional ages of the Dahongshan Formation at 273 and 261Ma, respectively.

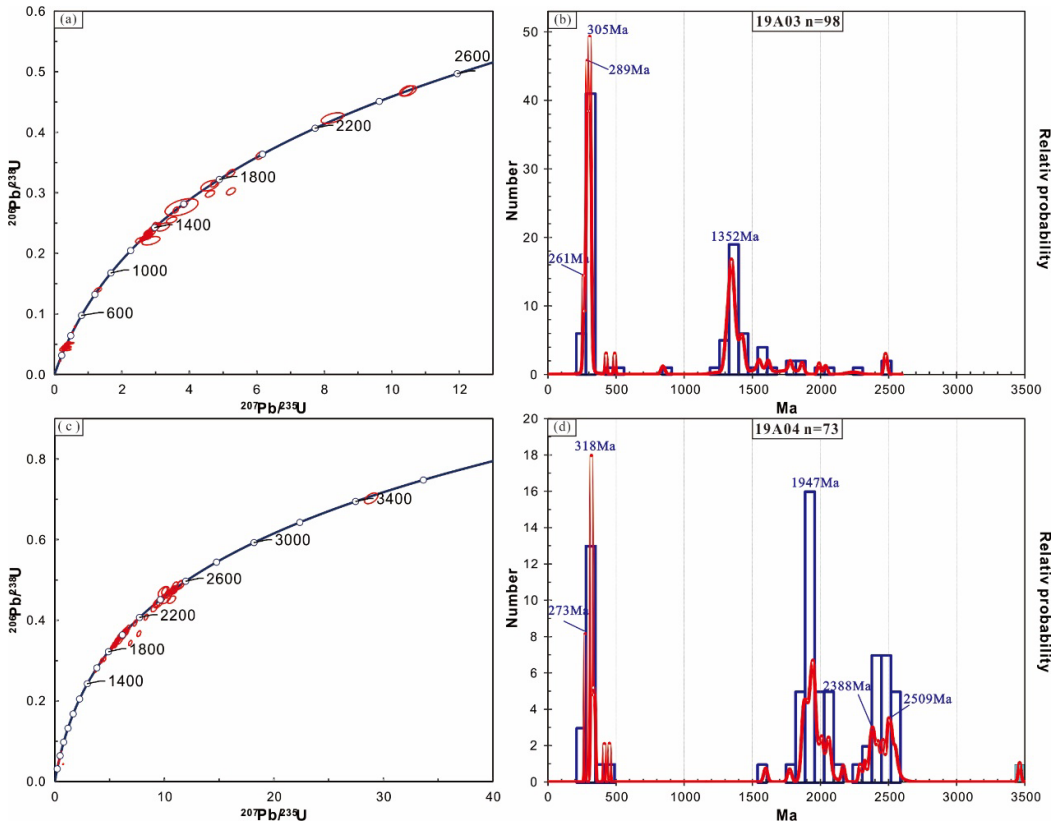

Figure 9. Concordia diagrams and age histograms of the detrital zircons from the Dahongshan Formation. Data with concordances between 90 and 110% are plotted.

5.2. Major and trace elements

Geochemical results for the Permian volcanic rocks in the Langshan belt are plotted in Fig. 10. Previous geochemical data of volcanic rocks from the Nuoergong – Langshan belt (Guo et al., 2017; Song et al., 2018b) are also plotted for comparison.

The Permian volcanic rocks in this study are intermediate to felsic with a wide range of SiO_2 contents (56.6–75.9 wt.%). The dacite and andesite show relatively high

LOI (loss on ignition, 2.2–5.0 wt. %), suggesting slight alteration or weathering. We thus use relatively immobile elements in the following discussion. In the Zr/TiO2 versus Nb/Y diagram, our samples are plotted in the andesite, dacite and rhyolite field (Fig. 10a), consistent with field and thin section observations (Fig. 7g, h and i). Chondrite–normalized REE patterns of these volcanic rocks are characterized by enrichments in the light rare earth elements (LREEs) relative to the heavy rare earth elements (HREEs), with La_n/Yb_n ratios of 9.78 – 14.12 and slightly negative Eu anomalies in the andesite and dacite (Eu/Eu* = 0.72 – 0.89) and significantly negative Eu anomalies (Eu/Eu* = 0.10 – 0.40) in the rhyolite (Fig. 10c; Table S2). The primitive–mantle normalized trace element diagram shows that these volcanic rocks are enriched in LILEs (e.g. K, Ba, Rb, and U) and depleted in HFSEs (e.g. Nb, Ta, P, and Ti) (Fig. 10d), typical for subduction–related magmas (Pearce and Peate. 1995).

6. Discussion

6.1. Sedimentary provenance and environment of the Permian strata

Before this study, no geochronology data have been reported for the Permian clastic sedimentary rocks in the Langshan region. Based on fossils and regional stratigraphic correlations, these clastic sediments were attributed to early Permian in age and named the Dahongshan Formation (BGMRNM. 1991). Detrital zircon U–Pb dating in this study suggests that the maximum depositional ages for samples 19A03

and 19A04 are 261Ma and 273Ma, respectively (Fig.9). A ca. 265Ma Zircon U-Pb age has been reported for volcanic rocks in the northern Langshan, which are probably correlative with the Dahongshan Formation (Guo et al., 2017). A significantly younger deposition age is unlikely considering the ubiquity of contemporary magmatic activity in this study area. Thus, the Dahongshan Formation is most likely deposited in the middle Permian (ca. 261 Ma).

The Dahongshan Formation shows a diverse lithology, including conglomerate, sandstone, slate, and minor limestone. Terrestrial plant fossils were also discovered in this formation (BGMRNM. 1991). The conglomerates contain pebbles with the diameter ranging from 2 mm to 50 cm and show poorly sorted characteristics (Fig. 7c), implying a short transportation distance and a proximal provenance from rapidly uplifting terranes. Detrital zircons from this formation are mainly composed of late Carboniferous to Permian and Palaeo–Mesoproterozoic grains (Fig. 9), suggesting denudation of relatively young magmatic rocks and ancient Precambrian basement. We compiled spectra in NLB. The age spectra of the Dahongshan Formation match well with the Paleozoic magmatic record and the Precambrian basement zircon ages (Fig. 11), consistent with a proximal source area for the Dahongshan Formation.

Different types of sedimentary basins may have distinct detrital zircon age distribution patterns. Generally, convergent settings are characterized by intense magmatic activities and therefore clastic sediments deposited in such tectonic settings contain a large proportion of zircon grains whose crystallization ages approximate the depositional age (Dickinson and Gehrels, 2009). In contrast, zircons from the

405 underlying ancient basement are more common in collisional and extensional settings.
406 Cawood et al. (2012) used detrital zircon age distribution patterns to identify tectonic
407 settings. According to this approach (Figure as supplementary materials), together
408 with the lithology and terrestrial plant fossils (BGMRNM. 1991), the Dahongshan
409 Formation was most likely deposited in a retroarc foreland basin, where pyroclastic
410 material with Carboniferous to Permian ages from the continental arc (see below) and
411 sediments eroded from the Alxa Precambrian basements were deposited (Fig. 14c).

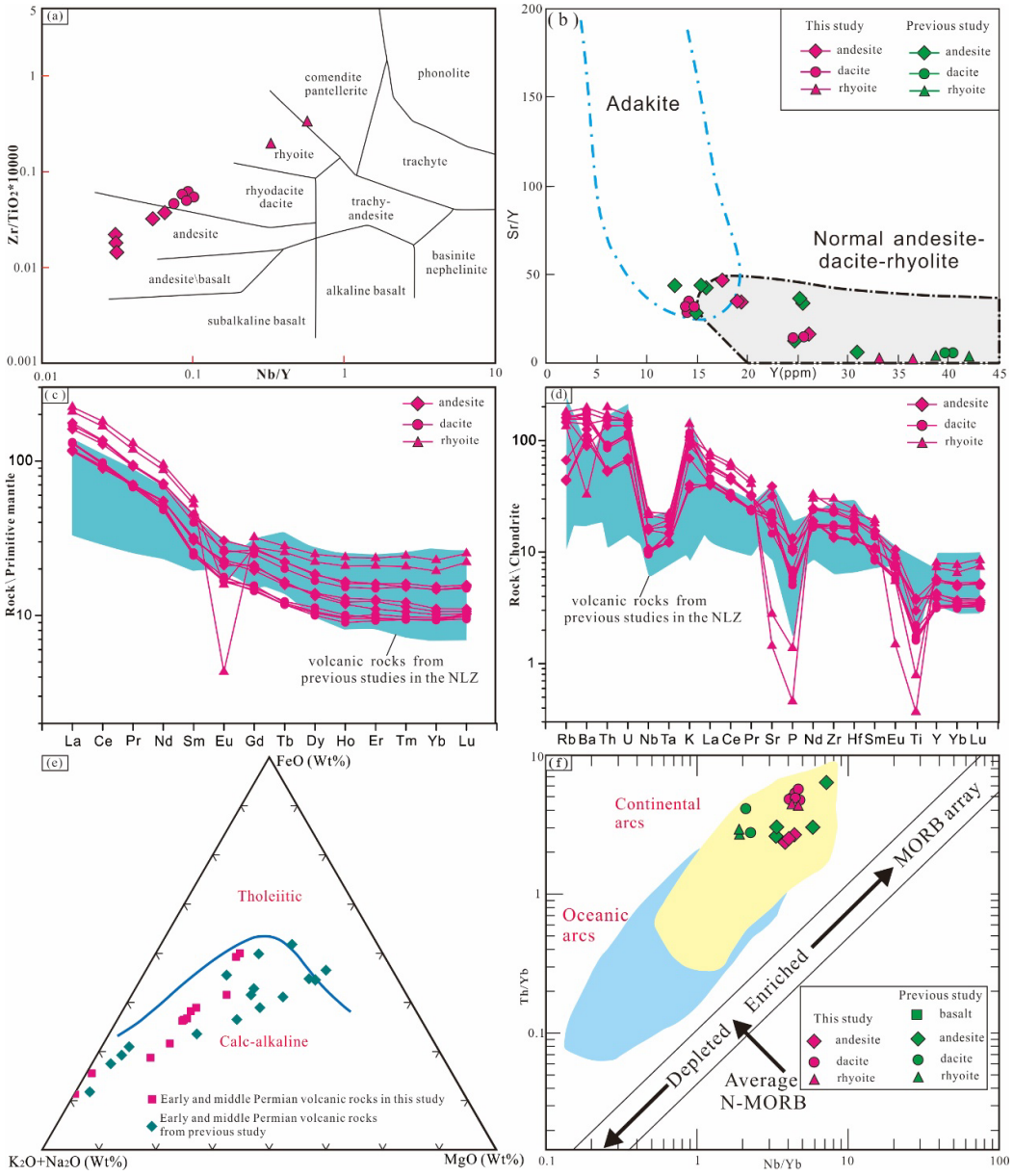

Figure 10. Geochemistry of the early and middle Permian volcanic rocks in the Nuoergong–Langshan zone. (a) Zr/TiO2 versus Nb/Y classification diagram after Winchester and Floyd, (1977); (b) Y versus Sr/Y diagram (after Defant and Drummond, 1993). (c) and (d) Chondrite - normalized rare earth element patterns and primitive mantle–normalized spider diagrams. Standardized values are from Sun and McDonough (1989). (e) AFM ternary diagram, after Irvine and Baragar, (1971). (f) Th/Yb–Nb/Yb diagram (after Pearce and Peate, 1995). Permian volcanic rocks from previous studies (Guo et al. 2017; Song et al. 2018b).

6.2 Tectonic setting of the Nuoergong–Langshan Zone during the Permian

The southernmost boundary of the CAOB in the Alxa Block has not been well constrained. Previous studies suggested that the ca. 300 Ma Enger Us ophiolite belt

represents the suture zone between the CAOB and the Alxa Block (Wang et al., 1998; Zheng et al., 2014; Xie et al., 2014), whereas the ca. 275 Ma Qagan Qulu ophiolite belt was interpreted as the location of final closure of a back–arc basin (Zheng et al., 2014). The early Permian volcanic and plutonic rocks in the Nuoergong–Langshan belt (NLB) were therefore interpreted to have been generated in a post–collisional setting or a mantle plume related extensional setting (Zhang et al., 2012; Dan et al., 2014b, 2015). Evidence supporting this model mainly includes: (1) a short period for the magmatic flare-up, (2) crust–mantle interaction, and (3) magmatic mixing. We discount this model, however, based on the following geological observations: (1) the early Permian plutons have a much smaller scale and span a longer interval (290–270 Ma) compared to large igneous province (Bryan and Ernst, 2008); (2) the presence of the Permian Qagan Qulu ophiolite belt in the northern part of this belt did not support a post–collisional setting (Zheng et al., 2014); (3) volcanic and plutonic rocks from this belt display cal–alkaline composition and arc–like geochemistry (Guo et al., 2017; Song et al., 2018b); and (4) intensive Permian folding and thrusting indicate a compressional setting.

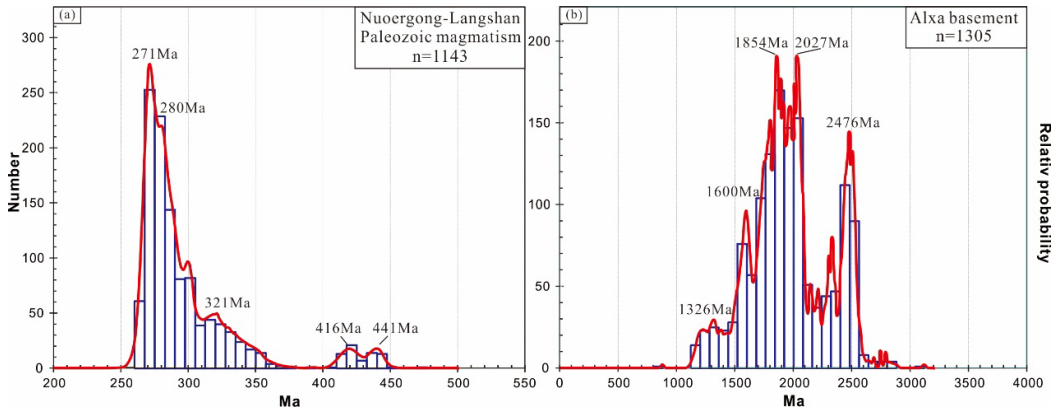

Figure 11. Compilation of zircon ages for (a) the Paleozoic magmatic rocks in the Nuoergong–Langshan zone and

(b) the Precambrian basement rocks of the Alxa Block. Data sources of the Paleozoic magmatic rocks in the Nuoergong–Langshan Zone are from (Liu et al. 2016b, 2017a, b; Dan et al. 2014b, 2016; Hu et al. 2015; Zhang et al. 2016b; Song et al. 2018b; Zheng et al. 2019a; Wang et al. 2015); data for the Alxa Precambrian basement rocks are from (Dan et al. 2012; Gong et al. 2012, 2016; Zhang et al. 2013b; Tian et al. 2019).

The early to middle Permian calc-alkaline volcanic rocks extend nearly 300 km along the Nuoergong-Langshan Belt (BGMRNM. 1991; Guo et al., 2017; Song et al., 2018b and this study). These volcanic rocks are characterized by relative enrichment of LILEs (e.g. K, Ba, Rb, and U) and LREE and depleted in HFSEs (e.g. Nb, Ta, P, and Ti) (Fig. 10d), indicating a subduction–related setting (Pearce and Peate. 1995). In the Th/Yb versus Nb/Yb discrimination diagram, all samples fall into the continental arc field (Fig. 10f), suggesting that the subduction of the PAO lasted at least to the early to middle Permian. The conclusion is also supported by geochemical data from Carboniferous to early Permian plutons in this belt (Shi et al., 2012; Peng et al., 2013; Liu et al., 2016a, 2017b; Song et al., 2018b; Zheng et al., 2019b). Song et al. (2018a) suggested that this belt probably extends eastward to the northern margin of the North China Craton, constituting an Andean–type magmatic arc along the northern margin of the Alax - NCC during the Carboniferous to middle Permian (Zhang et al., 2007a, 2009a, b; Liu et al., 2016a). The paucity of arc volcanic rocks probably results from intensive uplifting and denudation due to intraplate deformation, as documented in the Andean arcs (Ducea et al., 2015). In this context, the Permian mafic – ultramafic rocks (Feng et al., 2013), A–type and I–type granites (including high Sr/Y granodiorites) (Dan et al., 2014b), Adakitic rocks and Cu–Au mineralization (Li et al., 2010a, b) probably imply a slab window setting due to ridge subduction in the northern margin of the NLB.

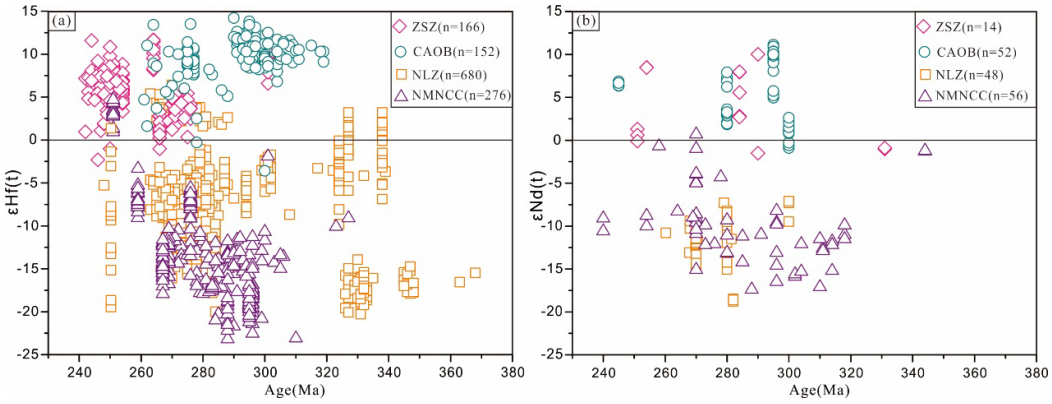

Figure 12. Compiled zircon Hf and whole–rock Nd isotopic compositions from Carboniferous to early Triassic plutons and volcanic rocks in the northern margin of the Alxa Block and adjacent regions. (a) Zircon Hf isotopic data are from (Shi et al. 2014a, b) for the Zongnaishan–Shalazhashan zone (ZSZ); (Zhang et al. 2018b, 2019; Shi et al. 2019; Wang et al. 2019) for the Central Asian Orogenic Belt (CAOB); (Pi et al. 2010; Peng et al. 2013; Hu et al. 2015; Liu et al. 2017a, b; Dan et al. 2014b, 2015; Liu et al. 2016a; Zheng et al. 2019a, b) for the Nuoergong–Langshan zone (NLZ); and (Ma et al. 2013; Zhang et al. 2007a, 2009a; Bai et al. 2013) for the North Margin of North China Craton (NMNCC). (b) Whole–rock Nd isotopic compositions in the ZSZ are from (Shi et al. 2018; Zhang et al. 2013a; Gan et al. 2018); the CAOB are from (Zhang et al. 2008, 2018b; Miao et al. 2008); the NLZ are from (Liu et al. 2017a; Dan et al. 2014b, 2015; Zheng et al. 2019a); and the NMNCC are from (Ma et al. 2013; Zhang et al. 2009a, b, 2016c; Ji et al. 2018).

It has been long proposed that the Zongnaishan–Shalazhashan zone (ZSZ) and Nuoergong–Langshan zone (NLZ) share similar basement and medium to high–grade metamorphism, and thus have a close tectonic affinity (e.g., Wang et al., 1994). However, the ca. 1.4 Ga Mesoproterozoic gneisses are the oldest documented basement rocks in the Zongnaishan area (Shi et al., 2016). In contrast, as part of the Alxa Block, the oldest basement rocks in the NLB are ca. 2.5 Ga TTG and Paleoproterozoic metamorphic complex (Dan et al., 2012; J.X. Zhang et al., 2013b; Gong et a., 2016), and ca. 1.4 Ga rocks are absent. More importantly, zircon Hf and whole–rock Nd isotopic compositions from the two belts differ significantly (Fig. 12). The ZSZ is characterized by juvenile isotopic compositions, comparable with those in the CAOB. Instead, the Carboniferous to early Triassic plutons and volcanic rocks from the NLZ have more negative zircon εHf and whole–rock εNd and are similar to

488 those from the northern margin of the NCC. We argue that the ZSZ and NLZ have
489 distinct Precambrian basement and Phanerozoic isotopic compositions and thus
490 constitute two separate tectonic units. The ZSZ likely represents a microcontinent
491 with the Mesoproterozoic basement in the CAOB. In fact, ca. 1.4 Ga magmatism has
492 been widely documented in micro–continent blocks of the CAOB, including the
493 central Tianshan Block (Hu et al., 2006; He et al., 2015a, 2018a), southern Beishan
494 (Liu et al., 2011; He et al., 2015b; Yuan et al., 2019), southern Mongolia (Demoux et
495 al., 2009) and the Xilinhot block (Han et al., 2017) but is rare in the Alxa Block and
496 NCC. Therefore, the southern boundary between the CAOB and Alxa Block is
497 probably the Qagan Qulu ophiolite, instead of the Enger Us ophiolite to the north.
498
499 **6.3. Folding and thrusting and its tectonic implications**
500
501 Accretionary orogens exhibit two distinct stress regimes and deformation
502 behaviors as exemplified as those in the western and eastern Pacific, respectively.
503 Cawood et al. (2009) grouped the accretionary orogens into the retreating and
504 advancing types. The advancing orogeny induces intensive compression, folding and
505 thrusting behind the arc (Stern. 2002; DeCelles. 2004; DeCelles et al., 2009; Ducea et
506 al., 2015), resulting in crustal shortening and thickening and formation of retroarc
507 foreland basins, as typified by the central Andes. In contrast, the retreating orogeny
508 generally results in pervasive extension and back-arc rifting or seafloor spreading
509 (Stern. 2002; Ducea et al., 2015).

510 During our field mapping, a large number of folds and thrusts were identified in
511 the NLZ. The NE-SW trending overturned isoclinal folds in the Diebusige Group and
512 the Langshan Group (Fig. 5b-f), as well as the large-scale southeastward thrusting
513 faults in the Permian granitic plutons (Fig. 5a), indicate an NW–SE compressional
514 deformation. Our previous study (Tian et al., 2017) indicated that these overturned
515 isoclinal folds were probably related to the evolution of the PAO. Zircon U-Pb dating
516 of folded felsic veins and unfolded intruding veins constrain the deformation age to
517 middle to late Permian (J. Zhang, unpublished). Andesite and dacite from the
518 Aguimiao area are characterized by high Sr (404-802 ppm), low Y (14.3-19.0 ppm)
519 and Yb (1.58-1.88 ppm) contents, relatively high Sr/Y ratios (28-47) and slightly
520 negative Eu anomaly and relatively low MgO contents (1.48-2.93 wt.%) (Table S2),
521 which are similar to those of Adakitic rocks (Fig. 10b) derived from melting of the
522 thickened mafic lower crust (Wang et al., 2006 and the references therein), supporting
523 extensive crustal thickening during the late Carboniferous to middle Permian.
524 Such thrusting and folding and crustal thickening might have been related to
525 oceanic ridge subduction (Feng et al., 2013), which has been widely recognized along
526 the southern margin of CAOB (Tang et al., 2010, 2012a, b; Zhang et al., 2018a; see
527 review in Windley et al. 2018).

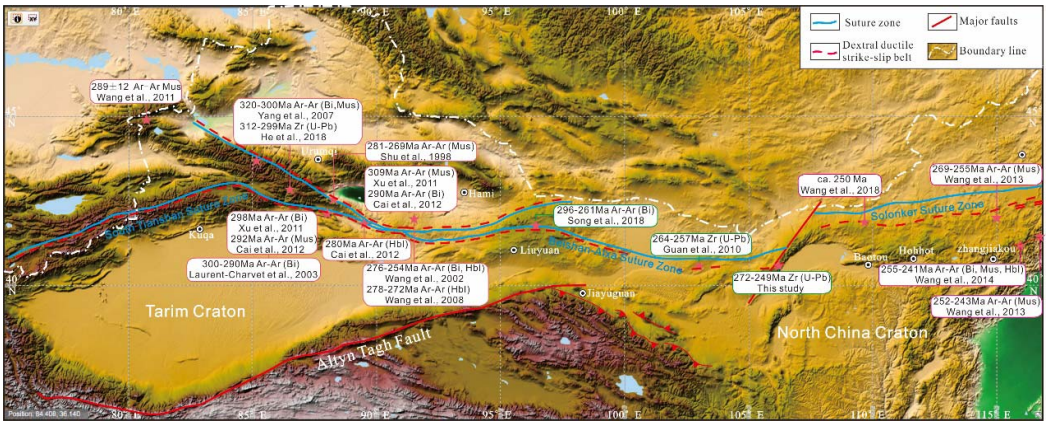

Figure 13. $^{40}Ar/^{39}Ar$ and zircon U–Pb dating constraint the dextral ductile strike–slip shearing in the south margin of CAOB, (background figure is downloaded from https://www.ngdc.noaa.gov/mgg/global/).

6.4. Timing of dextral strike–slip and its tectonic implications

The South Tianshan and Solonker suture zones are regarded as the locations of final subduction and closure of the PAO in the western and eastern parts of the southern CAOB, respectively. There is a consensus that the PAO closed in a scissor-like manner along the southernmost margin of the CAOB, with the closure time becoming younger from west to east, i.e. the late Carboniferous in the South Tianshan suture (Han et al., 2011; Klemd et al., 2015; Zhang et al., 2015a, 2016a; Wang et al., 2018a), the middle to late Permian in the Beishan and northern Alxa Block (Guo et al., 2012; Mao et al., 2012; Feng et al., 2013; Liu et al., 2017b, 2018a; Song et al., 2018a, b) and the Late Permian to Middle Triassic in the Solonker suture (Jian et al., 2010; Eizenhöfer et al., 2014; Eizenhöfer and Zhao et al., 2018).

Large–scale dextral strike–slip shear zone developed subparallel to the suture zone in the southern margin CAOB (Fig. 13). The deformation ages also become younger from the west to the east and are later than the final consumption of the PAO.

Based on field observations and isotopic dating over the last 20 years, the timing for the dextral strike–slip has been well constrained in the Tianshan belts (Fig. 13). In the western Tianshan, dextral ductile strike–slip may have initiated during 330–316 Ma (Wang et al., 2011). In the central Tianshan, dextral ductile shearing probably initiated at ca. 312–299 Ma (He et al., 2018b) and lasted to the early Permian (~270 Ma) (Shu et al., 1999; Laurent–Charvet et al., 2003; Yang et al., 2007; Xu et al., 2011a; Cai et al., 2012). Regional–scale dextral strike–slip zones in the eastern Tianshan formed during 290 – 272 Ma (Wang et al., 2008; Cai et al., 2012). Further west to the Kyrgyz western Tianshan, a late Carboniferous $^{40}Ar/^{39}Ar$ age of 312 Ma from a mylonite belt was regarded as the initiating age of dextral transpression and probably extended to the early Permian or middle Permian (Rolland et al., 2013).

In the middle section of southern CAOB, the Beishan orogenic belt underwent widespread ductile shearing deformation (Cai et al., 2012; Song et al., 2018c). Multiple ductile deformation events have been recorded by biotite $^{40}Ar–^{39}Ar$ ages of 323 ± 4 Ma, 296 ± 4 Ma, 261 ± 3 Ma in Beishan (Song et al., 2018c). Further east to the northern Alxa Block, Guan et al. (2010) constrained the deformation age between 264 Ma and 257 Ma based on zircon U – Pb dating of the mylonitic granite and the undeformed intruding diorite vein in the Tamusu area. In this study, our zircon U-Pb ages for the two granitic mylonites and the undeformed intruding diorite vein in the dextral shear zone constrain the deformation age between 272 Ma and 249 Ma.

In the eastern section of the southern margin of CAOB (i.e. northern margin of NCC), the dextral strike–slip has been constrained between 269 Ma and 241 Ma by

569 ^{40}Ar–^{39}Ar dating from the Fengning – Longhua and the Kangbao – Weichang fault
570 zone, in the Yinshan belt (Wang et al., 2013; Wang and Wan, 2014).

571 The large-scale strike-slip documented above may be akin to the present–day
572 southern Qinghai–Tibet Plateau where large scale strike–slip occurred subparallel to
573 the suture zone since the collision between the India block and Asia (Xu et al., 2011b).
574 This large-scale dextral strike–slip throughout the southern CAOB probably resulted
575 in eastward lateral extrusion of the thickened crust relative to the Tarim and North
576 China Craton after the continental collision (Wang et al., 2008, 2009, 2011 and this
577 study). Therefore, the final consumption of the PAO in the northern Alxa Block
578 probably occurred before this process in the middle to late Permian.

579

580 **6.5. Tectonic evolution of northern Alxa Block in late Paleozoic**

581

582 Based on the above discussion, we propose an updated model for the final stage
583 tectonic evolution of the PAO in the northern Alxa Block (Fig. 14).

584 During the early Carboniferous, the PAO subducted beneath the northern Alxa
585 Block, forming an active continent arc (Liu et al., 2016a; Zheng et al., 2019b). Similar
586 to microcontinents in the Central Tianshan and southern Beishan, the ZSZ is also
587 considered to be a microcontinent within the PAO, which finally amalgamated with
588 the northern ZHZ along the Enger Us suture zone at ca. 300 Ma (Zheng et al., 2014).
589 Late Carboniferous adakites was recognized in the ZHZ, providing evidence for the
590 subduction of the PAO (Shi et al., 2014a).

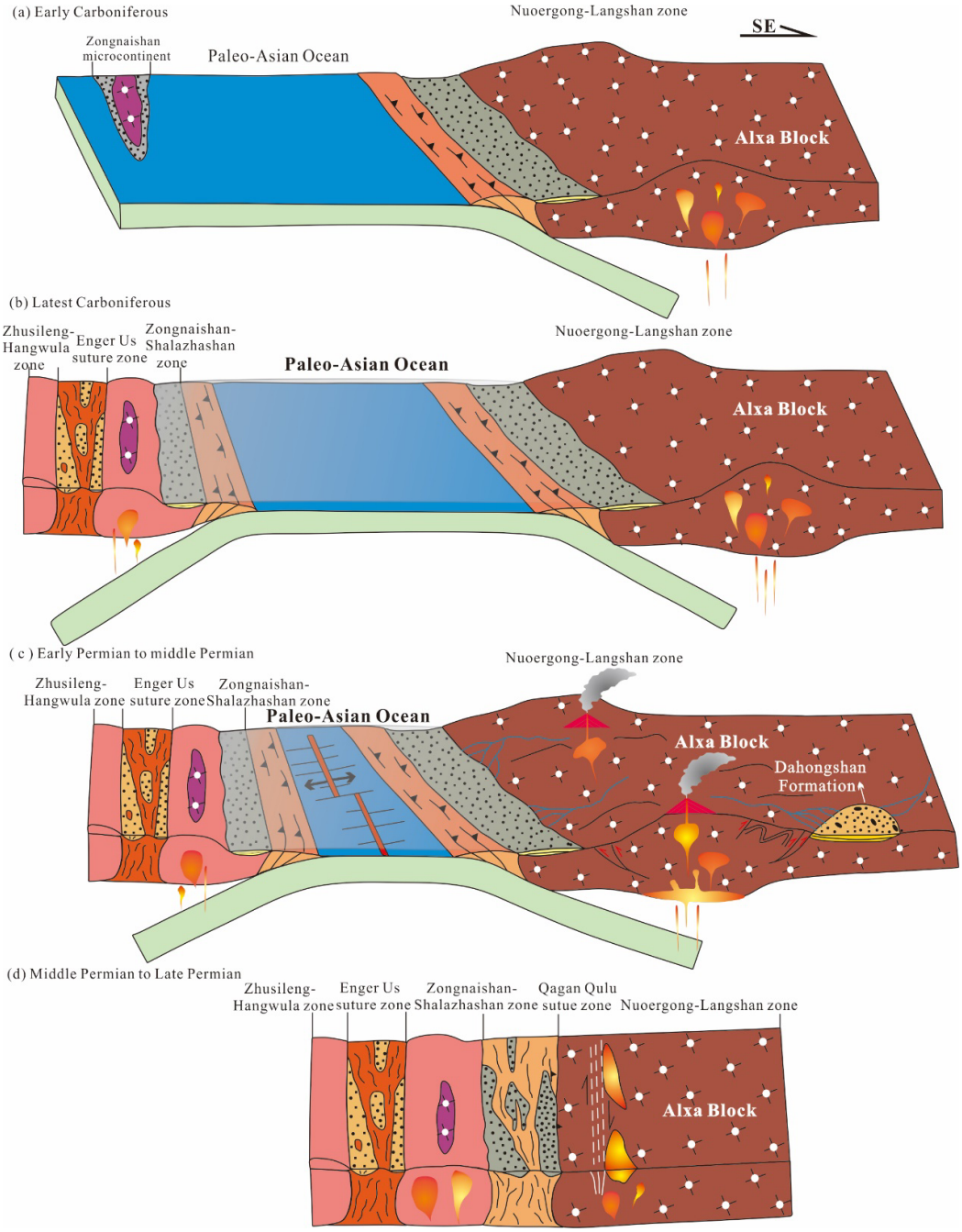

Figure 14. Schematic tectonic evolution for the northern Alxa Block relating to the final consumption of the Paleo-Asian Ocean (PAO). (a) The PAO subducted southeastward beneath the Alxa Block during the early Carboniferous; (b) the Zongnaishan–Shalazhashan microcontinent amalgamated with the Zhusileng–Hangwula arc along the Enger Us suture zone during the latest Carboniferous; (c) divergent double subduction of the PAO resulted in NW–SE compression during the early – middle Permian; (d) final closure of the PAO took place along the Qagan Qulu suture zone during the middle to late Permian, resulting in large-scale dextral strike–slip and eastward extrusion of the Central Asian Orogenic Belt.

In the early to middle Permian, the PAO started to diminish and close due to double–sided subduction. This led to widespread arc magmatism peaking at ca. 280–270 Ma in the NLZ and ZSZ (Yang et al., 2014; Dan et al., 2014b, 2015; J.J Zhang et al., 2016b; Zheng et al., 2019a and this study). Carboniferous to Permian arc-related volcanic rocks and sedimentary rocks (i.e. the Amushan Formation) are widespread along both sides of the Qagan Qulu suture zone (W. Zhang et al., 2013a; Zheng et al., 2017). During the middle to late Permian, an oceanic ridge within the PAO subducted beneath the Alxa Block (Feng et al., 2013), resulting in the collision between the ZSZ and the NLZ and forming the intervening Qagan Qulu suture zone. This also induced thrusting and folding and formation of a retroarc foreland basin, within which the Dahongshan Formation deposited. The Qagan Qulu suture zone in the Alxa Block probably marks the final closure of the PAO in the middle segment of the southern CAOB and is probably comparable with the Solonker suture zone to the east (Song et al., 2018a). After the collision, large-scale dextral ductile shear zones occurred, resulting in eastward lateral extrusion of the CAOB. We thus argue that the final consumption of the PAO occurred during the middle – later Permian in the northern Alxa Block.

7. Conclusions

(1) A ~300 km volcanic belt is identified in the Nuoergong – Langshan zone, which includes dacite, andesite, and rhyolite emplaced between 273 Ma and 263 Ma.

These rocks show cal–alkaline characteristics with enrichments of LILEs and depletion of HFSEs, indicating a continental arc environment.

(2) The PAO subducted southeastward along the northern Alxa Block in the early to middle Permian, resulting in NW-SE compression and large-scale folding and thrust faulting and crustal thickening in the Nuoergong-Langshan zone.

(3) The Dahongshan Formation mainly contains Carboniferous to Permian and Mesoproterozoic to Paleoproterozoic detrital zircons and probably had a proximal provenance from rapidly uplifting terranes, suggesting deposition in a back-arc foreland basin shortly after ~261 Ma.

(4) Large-scale dextral strike-slip occurred in the Langshan zone, which is constrained to take place between 272 Ma and 249 Ma using zircon U–Pb dating.

(5) Collectively, our data indicate that the final consumption of the PAO occurred in the middle – late Permian along the Qagan Qulu suture zone in the northern Alxa Block.

Acknowledgments

We have begun archiving our data in appropriate repositories, and the data archiving is underway. We plan to archive our Supplementary Material in the *4TU.Centre for Research Data*. Data and analytical methods for this article are either included as supporting information. We are grateful to Rongfeng Ge for his constructive comments and improvements on an early version of the manuscript. Special thanks are given to our team members (Qinglong Zhang, Junfeng Qu, Amirdin

644 Aierkin, Fahao Li and Pengfei Niu) for their assistance and patient guidance during
645 field mapping. We also appreciate the assistance of Ziman Wu in an earlier version of
646 the draft. This study was supported by the National Key R&D Plan of China (Grant
647 Nos. 2017YFC0601402 and 2018YFC0603703).

648

649 **References**

650

651 Bai, X., Liu, S., Wang, W., Yang, P., Li, Q., 2013. U – Pb geochronology and Lu – Hf isotopes of zircons from
652 newly identified Permian – Early Triassic plutons in western Liaoning province along the northern margin of
653 the North China Craton: Constraints on petrogenesis and tectonic setting. International Journal of Earth
654 Sciences 102, 671 – 685.

655 Bryan, S.E., Ernst, R.E., 2008. Revised definition of large igneous provinces (LIPs). Earth–Science Reviews 86,
656 175 – 202.

657 Bureau of Geology and Mineral Resources of Nei Mongol Autonomous Region, BGMRNM (1982). Investigation
658 report of regional geology in Shandaoqiao region, China (in Chinese). P36–39 (In Chinese).

659 Bureau of Geology and Mineral Resources of Nei Mongol Autonomous Region, BGMRNM (1991). Regional
660 geology of Nei Mongol Autonomous Region (in Chinese) (p. 725). Beijing: Geological Publishing House
661 (In Chinese).

662 Cai, Z.H., Xu, Z.Q., He, B.Z., Wang, R.R., 2012. Age and tectonic evolution of ductile shear zone in the eastern
663 Tianshan–Beishan orogenic belt. Acta Petrologica Sinica, 28(6): 1875–1895 (In Chinese with English
664 abstract).

665 Cawood, P. A., Kröner, A., Collins, W. J., Kusky, T. M., Mooney, W. D., Windley, B. F., 2009. Accretionary

orogens through Earth history. Geological Society, London, Special Publications, 318, 1 – 36.

Cawood, P.A., Hawkesworth, C.J., Dhuime, B., 2012. Detrital zircon record and tectonic setting. Geology 40:875 – 878

Demoux, A., Kröner, A., Liu, D., Badarch, G., 2009. Precambrian crystalline basement in southern Mongolia as revealed by SHRIMP zircon dating. Internal Journal of Earth Science 98, 1365–1380.

Dan, W., Li, X.H., Guo, J., Liu, Y., Wang, X.C., 2012. Paleoproterozoic evolution of the eastern Alxa Block, westernmost North China: evidence from in situ zircon U–Pb dating and Hf–O isotopes. Gondwana Research 21 (4), 838–864.

Dan, W., Li, X.–H., Wang, Q., Wang, X.–C., Liu, Y., 2014a. Neoproterozoic S–type granites in the Alxa Block, westernmost North China and tectonic implications: in situ zircon U–Pb–Hf–O isotopic and geochemical constraints. American Journal of Science 314 (1), 110–153.

Dan, W., Li, X. H., Wang, Q., Tang, G.J., Liu, Y., 2014b. An Early Permian (ca. 280 Ma) silicic igneous province in the Alxa Block, NW China: a magmatic flare–up triggered by a mantle–plume? Lithos 204, 144 – 158.

Dan, W., Wang, Q., Wang, X. C., Liu, Y., Wyman, D. A. & Liu, Y. S. (2015). Overlapping Sr–Nd–Hf–O isotopic compositions in Permian mafic enclaves and host granitoids in Alxa Block, NW China: Evidence for crust–mantle interaction and implications for the generation of silicic igneous provinces. Lithos 230, 133–145.

Dan, W., Li, X.H., Wang, Q., Wang, X.C., Wyman, D.A., Liu, Y., 2016. Phanerozoic amalgamation of the Alxa Block and NCC: evidence from Paleozoic granitoids, U–Pb geochronology and Sr–Nd–Pb–Hf–O isotope geochemistry. Gondwana Research http://dx.doi.org/10.1016/j.gr.2015.02.011.

Defant, M.J., Drummond, M.S., 1993. Mount St. Helens; potential example of the partial melting of the subducted lithosphere in a volcanic arc. Geology 21, 547 – 550.

DeCelles PG. 2004. Late Jurassic to Eocene evolution of the Cordilleran thrust belt and foreland basin system,

688 western U.S.A. America Journal of Science 304:105–68

689 DeCelles, P. G., Ducea, M. N., Kapp, P., Zandt, G., 2009. Cyclicity in Cordilleran orogenic systems. Nature

690 Geoscience 2, 251–257.

691 Dickinson, W.R., Gehrels, G.E., 2009. Use of U–Pb ages of detrital zircons to infer maximum depositional ages of

692 strata: a test against a Colorado Plateau Mesozoic database. Earth and Planetary Science Letter 288:115–

693 125

694 Ducea, M.N., Saleeby, J.B., and Bergantz, G., 2015. The Architecture, Chemistry, and Evolution of Continental

695 Magmatic Arcs: Annual Review of Earth and Planetary Sciences 43, 299–331

696 Eizenhöfer, P.R., Zhao, G., Zhang, J., Sun, M., 2014. Final closure of the Paleo–Asian Ocean along the Solonker

697 Suture Zone: constraints from geochronological and geochemical data of Permian volcanic and sedimentary

698 rocks. Tectonics 33 (4), 441–463.

699 Eizenhöfer, P.R., Zhao, G., 2018. Solonker Suture in East Asia and its bearing on the final closure of the eastern

700 segment of the Palaeo–Asian Ocean. Earth–Science Review 186, 153–172.

701 Feng, J. Y., Xiao, W. J., Windley, B. F., Han, C. M., Wan, B., Zhang, J. E., et al. (2013). Field geology,

702 geochronology and geochemistry of mafic–ultramafic rocks from Alxa, China: Implications for Late

703 Permian accretionary tectonics in the southern Altaids. Journal of Asian Earth Sciences, 78, 114–142.

704 https://doi.org/10.1016/j.jseaes.2013.01.020.

705 Gan, L.S., Wu, T.R., Chen, Y., Zhang, W., Zhang, Z.Y., 2018. Geochronology and geochemical characteristics of

706 the Shangdan pluton in the northern margin of the Alxa Block，Inner Mongolia and its tectonic implications.

707 Acta Petrologica Sinica，34(11): 3359–3374 (In Chinese with English abstract).

708 Gong, J.H., Zhang, J.X., Yu, S.Y., Li, H.K., Hou, K.J., 2012. ~2.5 Ga TTG gneiss and its geological implications

709 in the western Alxa Block, North China Craton. Chinese Science Bulletin 57, 4064–4076 (In Chinese with

English abstract).

Gong, J.H., Zhang, J.X., Wang, Z.Q., Yu, S.Y., Li, H.K., Li, Y.S., 2016. Origin of the Alxa Block, western China: New evidence from zircon U–Pb geochronology and Hf isotopes of the Longshoushan Complex. Gondwana Research 36, 359–375.

Gong, W.B., Hu, J.M., Wu, S.J., Liu, Y., Zhao, Y.F., 2017. Deformation characteristics, timing and significance of the Langshan sinistral strike–slip ductile shear zone, Inner Mongolia, Earth Science Frontiers, 24(3):263–275 (in Chinese with English abstract).

Guan, J., 2010. Study of the Aergashun ductile shear zone in Tamusu region of Alxa Youqi, Inner Mongolia. Master Dissertation of China University of Geoscience, P1–57 (in Chinese with English abstract).

Guo, Q. Q., Xiao, W. J., Windley, B. F., Mao, Q. G., Han, C. M., Qu, J. F., et al. (2012). Provenance and tectonic settings of Permian turbidites from the Beishan Mountains, NW China: Implications for the Late Paleozoic accretionary tectonics of the southern Altaids. Journal of Asian Earth Sciences, 49, 54 – 68. https://doi.org/10.1016/j.jseaes.2011.03.013.

Guo, S., Teng, X.J., Liu, Y., Teng, F., He, P., Wang, W.L., Tian, J., Duan, X.L., 2017. Geochemistry, chronology and Hf isotope features of the Permian intermediate–basic volcanic rocks in Wulanaobao area, Urad Houqi, Inner Mongolia and its geological significance. Journal of Geomechanics, 23:397–410 (in Chinese with English abstract).

Han, B. F., Zhang, C., Zhao, L., Ren, R., Xu, Z., Chen, J. F., Zhang, L., Zhou, Y. Z., Song, B., 2010. A preliminary study of granitoids in western Inner Mongolia. Acta Petrol. Mineral. 29:741–749 (in Chinese with English abstract).

Han, B.F., He, G.Q., Wang, X.C., Guo, Z.J., 2011. Late Carboniferous collision between the Tarim and Kazakhstan–Yili terranes in the western segment of the South Tian Shan Orogen, Central Asia, and

implications for the Northern Xinjiang, western China. Earth Sci. Rev. 109, 74 – 93. http://dx.doi.org/10.1016/j.earscirev.2011.1009.1001.

Han, J., Zhou, J.B., Li, L., Song, M.C., 2017. Mesoproterozoic (~1.4 Ga) A–type gneissic granites in the Xilinhot terrane, NE China: first evidence for the break–up of Columbia in the eastern CAOB. Precambrian Research 296, 20 – 38.

He, Z.Y., Klemd, R., Zhang, Z.M., Zong, K.Q., Sun, L.X., Tian, Z.L., Huang, B.T., 2015a. Mesoproterozoic continental arc magmatism and crustal growth in the eastern Central Tianshan Arc Terrane of the southern Central Asian Orogenic Belt: geochronological and geochemical evidence. Lithos 236 – 237, 74 – 89.

He, Z.Y., Sun, L.X., Mao, L.J., Zong, K.Q., Zhang, Z.M., 2015b. Zircon U–Pb and Hf isotopic study of the gneiss and granodiorite from the southern Beishan orogenic collage: Mesoproterozoic magmatism and crustal growth. Chin. Sci. Bull. 60, 389 – 399 (in Chinese with English abstract).

He, Z.Y., Klemd, R., Yan, L.L., Lu, T.Y., Zhang, Z.M., 2018a. Mesoproterozoic juvenile crust in micro–continents of the Central Asian Orogenic Belt: evidence from oxygen and hafnium isotopes in zircon. Science Reports. 8, 5054.

He, Z.Y., Wang, B., Zhong, L.L., Zhu, X.Y., 2018b. Crustal evolution of the Central Tianshan Block: Insights from zircon U–Pb isotopic and structural data from meta–sedimentary and meta–igneous rocks along the Wulasitai – Wulanmoren shear zone. Precambrian Research 314, 111–128.

Hu, A.Q., Wei, J.G., Deng, W.F., Zhang, J.B., Chen, L.L., 2006. 1.4 Ga SHRIMP U–Pb age for zircons of granodiorite and its geological significance from the eastern segment of the Tianshan Mountains, Xinjiang, China. Geochemistry 35, 333 – 345 (in Chinese with English abstract).

Hu, J.M., Gong, W.B., Wu, S.J., Liu, Y., Liu, S.C., 2014. LA–ICP–MS zircon U–Pb dating of the Langshan Group in the northeast margin of the Alxa Block, with tectonic implications. Precambrian Research 255 (Part 2, no.

754 0), 756–770.

755 Hu, C.S., Li, W.B., Xu, C., Zhong, R.C., Zhu, F., Qiao, X.Y., 2015. Geochemistry and petrogenesis of Permian
756 granitoids in the northwestern margin of the North China Craton: insights from the Dongshengmiao pluton,
757 Inner Mongolia, International Geology Review, 57:14, 1843–1860, DOI: 10.1080/00206814.2015.1039087

758 Irvine, T.N., Baragar, W.R.A., 1971. A guide to the chemical classification of the common volcanic rocks. Can. J.
759 Earth Sci. 8, 523 – 548. https://doi.org/10.1139/e71–055.

760 Ji, Z.J., Zhang, Z.C., Chen, Y., Li, K., Yang, J.F., Qian, X.Y., 2018. Geochemistry, geochronology, and Sr–Nd
761 isotopic compositions of Permian volcanic rocks in the northern margin of the North China Block:
762 implications for the tectonic setting of the southeastern Central Asian Orogenic Belt: International Journal of
763 Earth Sciences, 107, 2143–2161.

764 Jian, P., Liu, D., Kröner, A., Windley, B.F., Shi, Y., Zhang, W., Tomurhuu, D., 2010. Evolution of a Permian
765 intraoceanic arc – trench system in the Solonker suture zone, Central Asian Orogenic Belt, China and
766 Mongolia. Lithos 118 (1), 169 – 190.

767 Klemd, R., Gao, J., Li, J.L., and Meyer, M., 2015, Metamorphic evolution of (ultra)–high–pressure subduction–
768 related transient crust in the South Tianshan orogen (Central Asian orogenic belt): Geodynamic implications:
769 Gondwana Research, v. 28, p. 1–25, https://doi .org/10.1016/j.gr.2014.11.008.

770 Laurent–Charvet, S., Charvet, J., Monié, P., Shu, L.S., 2003. Late Paleozoic strike–slip shear zones in eastern
771 central Asia (NW China): new structural and geochronological data. Tectonics 22, 1009. doi:
772 10.1029/2001TC901047.

773 Le Maitre, R., Bateman, P., Dudek, A., Keller, J., Lameyre, J., Le Bas, M., Sabine, P., Schmid, R., Sorensen, H.,
774 Streckeisen, A., 1989. A classification of igneous rocks and glossary of terms. Recommendations of the
775 IUGS Subcommission on the Systematics of Igneous rocks. Blackwell Scientific Publications, London.

776 Li, J. J., Zhai, Y. S., Sang, H. Q., Li, H. M., Zhang, Y. S., Liu, S. Y., Wang, S. G., Sun, Z. P., Liu, X. Y., 2010a.
777 Metallogenic Epoch of the Oubulage Copper–Gold Deposit in the Alashan Area, Inner Mongolia
778 Autonomous Region. Bulletin of Mineralogy, Petrology and Geochemistry 29 (4):323–327 (in Chinese with
779 English abstract).
780 Li, J. J., Zhai, Y. S., Yang, Y. Q., Wang, Y. B., Li, C. D., Cui, L. W., Zhou, H. Y., Liu, X. Y., Liu, X. X., Li. S.,
781 2010b. Re–discussion on the metallogenic age of Zhulazaga gold deposit in Alashan area, Inner, Mongolia:
782 Evidence from zircon U–Pb SHRIMP age. Earth Science Frontiers 17 (2) 178–184 (in Chinese with English
783 abstract).
784 Li, J.Y., Zhang, J., Qu, J.F., 2012. Amalgamation of North Craton with Alxa Block in the late of Early Paleozoic:
785 evidences from sedimentary sequences in the Niushou Mountain, Ningxia Hui Autonomous Region, NW
786 China. Geological Review 58, 208 – 214 (in Chinese with English abstract).
787 Liu, M., Zhang, D., Xiong, G., Zhao, H., Di, Y., Wang, Z., Zhou, Z., 2016a. Zircon U–Pb age, Hf isotope and
788 geochemistry of Carboniferous intrusions from the Langshan area, Inner Mongolia: Petrogenesis and
789 tectonic implications. Journal of Asian Earth Sciences 120, 139–158.
790 Liu, Q., Zhao, G. C., Sun, M., Han, Y. G., Eizenhöfer, P. R., Hou, W. Z., Zhang, X. R., Zhu, Y.L., Wang, B., Liu,
791 D.X., Xu, B., 2016b. Early Paleozoic subduction processes of the Paleo–Asian Ocean: insights from
792 geochronology and geochemistry of Paleozoic plutons in the Alxa Terrane. Lithos 262:546–560.
793 Liu, Q., Zhao, G.C., Han, Y.G., Eizenhöfer, P.R., Zhu, Y.L., Hou, W.Z., and Zhang, X.R., 2017a, Timing of the
794 final closure of the Paleo–Asian Ocean in the Alxa terrane: Constraints from geochronology and
795 geochemistry of late Carboniferous to Permian gabbros and diorites: Lithos, 274–275: 19–30,
796 https://doi.org/10.1016/j. lithos.2016.12.029.
797 Liu, Q., Zhao, G., Han, Y., Eizenhöfer, P.R., Zhu, Y., Hou, W., Zhang, X., and Wang, B., 2017b. Geochronology

and geochemistry of Permian to Early Triassic granitoids in the Alxa Terrane: Constraints on the final closure of the Paleo–Asian Ocean: Lithosphere, 9(4):665–680.

Liu, Q., Zhao, G.C., Han, Y.G., Zhu, Y.L., Wang, B., Eizenhöfer, P.R., Zhang, X.R., Tsui, R.W.S., 2018a. Timing of the final closure of the middle segment of the Paleo–Asian Ocean: Insights from geochronology and geochemistry of Carboniferous –Triassic volcano–sedimentary successions in western Inner Mongolia, China. GSA Bulletin 131 (5–6): 941–965. https://doi.org/10.1130/B32023.1

Liu, Q., Zhao, G., Han, Y., Li, X., Zhu, Y., Eizenhöfer, P.R., Zhang, X., Wang, B., Tsui, R.W., 2018b. Geochronology and Geochemistry of Paleozoic to Mesozoic Granitoids in Western Inner Mongolia, China: Implications for the Tectonic Evolution of the Southern Central Asian Orogenic Belt. The Journal of Geology126, 451–471.

Ma, X., Chen, B., Chen, J. F., Niu, X.L., 2013. Zircon SHRIMP U–Pb age, geochemical, Sr–Nd isotopic, and in–situ Hf isotopic data of the Late Carboniferous–Early Permian plutons in the northern margin of the North China Craton. Science China: Earth Sciences, 56: 126–144, doi: 10.1007/s11430–012–4456–6

Mao, Q.G., Xiao, W.J., Fang, T.H., Wang, J.B., Han, C.M., Sun, M., Yuan, C., 2012. Late Ordovician to early Devonian adakites and Nb–enriched basalts in the Liuyuan area, Beishan, NW China: implications for early Paleozoic slab–melting and crustal growth in the southern Altaids. Gondwana Research 22, 534–553

Pearce JA, Peate DW. 1995. Tectonic implications of the composition of volcanic arc magmas. Annual Review of Earth Planetary Science. 23:251–86

Peng, R.M., Zhai, Y.S., Li, C.S., Ripley, E.M., 2013. The Erbutu Ni–Cu deposit in the Central Asian Orogenic Belt: a Permian magmatic sulfide deposit related to boninitic magmatism in an arc setting. Economic Geology 108, 1879–1888.

Pi, Q.H., Liu, C.Z., Chen, Y.L., Li, Y.Q., Li, D.P., 2010. Formation epoch and genesis of intrusive rocks in

820 Huogeqi ore field of Inner Mongolia and their relationship with copper mineralization. Mineral Deposits 29,
821 437–451 (in Chinese with English abstract).
822 Ren, K.X., Yan, G.H., Mu, B.L., Cai, J.H., Tong, Y., Li, F.T., Zhao, F.S., Gu, L.B., Yang, B., Chu, Z.Y., 2005
823 Geochemistry and Nd, Sr , Pb isotopic characteristics of the alkali–rich intrusive rocks in Alxa Fault Block,
824 Western Inner Mongolia and their implications. Earth Science Frontiers, 2005, 12(2):292–301 (in Chinese
825 with English abstract).
826 Rolland, Y., Alexeiev, D.V., Kröner, A., Corsini, M., Loury, C., Monié, P., 2013. Late Palaeozoic to Mesozoic
827 kinematic history of the Talas–Ferghana strike–slip fault (Kyrgyz West Tianshan) as revealed by 40Ar/39Ar
828 dating of syn–kinematic white mica. Journal of Asian Earth Science 67–68, 76–92.
829 Şengör A.M.C, Natal'in BA, Burtman VS. 1993. Evolution of the Altaid tectonic collage and Palaeozoic crustal
830 growth in Eurasia. *Nature* 364:299–307
831 Şengör, A.M.C., Natal' In, B.A., Sunal, G., van der Voo, R., 2018. The Tectonics of the Altaids: Crustal Growth
832 during the Construction of the Continental Lithosphere of Central Asia Between ~750 and ~130 Ma Ago.
833 Annual Review of Earth and Planetary Sciences 46, 439–494.
834 Shi, X. J., Tong, Y., Wang, T., Zhang, J. J., Zhang, Z. C., Zhang, L., Guo, L., Zeng, T. Geng, J. Z. (2012). LA–
835 ICP–MS zircon U–Pb age and geochemistry of the Early Permian Halinudeng granite in northern Alxa area,
836 western Inner Mongolia. Geological Bulletin of China 31, 662–670 (in Chinese with English abstract).
837 Shi, X.J., Wang, T., Zhang, L., Castro, A., Xiao, X.C., Tong, Y., Zhang, J.J., Guo, L., Yang, Q.D., 2014a. Timing,
838 petrogenesis and tectonic setting of the Late Paleozoic gabbro–granodiorite–granite intrusions in the
839 Shalazhashan of northern Alxa: constraints on the southernmost boundary of the Central Asian Orogenic
840 Belt. Lithos 208–209,158–177.
841 Shi, X. J., Zhang, L., Wang, T., Xiao, X. C., Tong, Y., Zhang, J. J., Geng, J. Z., Ye, K., 2014b. Geochronology and

842 geochemistry of the intermediate–acid intrusive rocks from Zongnaishan area in northern Alxa, Inner
843 Mongolia, and their tectonic implications. Acta Petrol. Mineral. 33:989–1007 (in Chinese with English
844 abstract).
845 Shi, X.J., Zhang, L., Wang, T., Zhang, J.J., Liu, M.H., Zhou, H.S., Yan, Y.T., 2016. Zircon geochronology and Hf
846 isotopic compositions for the Mesoproterozoic gneisses in Zongnaishan area, northern Alxa and its tectonic
847 affinity. Acta Petrol Sin. 32, 3518–3536 (in Chinese with English abstract).
848 Shi, G. Z., Wang, H., Liu, E. T., Huang, C. Y., Zhao, J. X., Song, G. Z., Liang, C., 2018. Sr–Nd–Pb isotope
849 systematics of the Permian volcanic rocks in the northern margin of the Alxa Block (the Shalazhashan Belt)
850 and comparisons with the nearby regions: Implications for a Permian rift setting? Journal of Geodynamics
851 115, 43–56.
852 Shi, Y., Yao, Y., Liu, Z.H., Liu, J., Wei, M.H., Gu, Y.C., Yang, F., Zhang, L., and Shi, S.S., 2019.
853 Petrogeochemical characteristics, zircon SHRIMP U–Pb ages and Lu–Hf isotopic compositions of Late
854 Carboniferous A–type granitoids, Yili area, Inner Mongolia (China). Geological Journal, 54(2): 770–790.
855 Shu, L.S., Charvet, J., Guo, L.Z., Lu, H.F., Laurent–Charvet, S., 1999. A large–scale Paleozoic dextral ductile
856 strike–slip zone: the Aqqikkudug–Weiya zone along the northern margin of the Central Tianshan belt,
857 Xinjiang, NW China. Acta Geologica Sinica 73 (2), 148–162 (In Chinese with English abstract).
858 Song, D., Xiao, W., Collins, A.S., Glorie, S., Han, C., Li, Y., 2018a. Final Subduction Processes of the Paleo–
859 Asian Ocean in the Alxa Tectonic Belt (NW China): Constraints from Field and Chronological Data of
860 Permian Arc–Related Volcano–Sedimentary Rocks. Tectonic 37, 1658–1687.
861 Song, D., Xiao, W., Collins, A., Glorie, S., Han, C., 2018b. Late Carboniferous–early Permian arc magmatism in
862 the south–western Alxa Tectonic Belt (NW China): Constraints on the late Palaeozoic subduction history of
863 the Palaeo–Asian Ocean. Geological Journal. 2018, 1–18.

Song, D.F., Xiao, W.J., Han, C.M., Tian, Z.H., Li, Y.C., 2018c. Accretionary processes of the central segment of Beishan: Constraints from structural deformation and 40Ar–39Ar geochronology. Acta Petrologica Sinica，34(7) : 2087–2098 (In Chinese with English abstract).

Stern, R. J., 2002. Subduction zones. Reviews of Geophysics, 40(4), 1012, doi: 10.1029/2001RG000108, 2002.

Sun, S.S., McDonough, W.F., 1989. Chemical and isotopic systematic of oceanic basalts: implications for mantle composition and processes. In: In: Saunders, A.D., Norry, M.J. (Eds.), Magmatism in the Oceanic Basins, vol. 42. Geological Society of London, pp.313 – 345.

Tang, G.J., Wang, Q., Wyman, D.A., Li, Z.X., Zhao, Z.H., Jia, X.H., Jiang, Z.Q., 2010. Ridge subduction and crustal growth in the Central Asian Orogenic Belt: evidence from Late Carboniferous adakites and high–Mg diorites in the western Junggar region, northern Xinjiang (west China). Chemical Geology 277, 281–300.

Tang, G.J., Wang, Q., Wyman, D.A., Li, Z.X., Zhao, Z.H., Yang, Y.H., 2012a. Late Carboniferous high εNd(t) – εHf(t) granitoids, enclaves and dikes in western Junggar, NW China: ridge–subduction–related magmatism and crustal growth. Lithos 140, 86 – 102.

Tang, G.J., Wyman, D.A., Wang, Q., Li, J., Li, Z.X., Zhao, Z.H., Sun, W.D., 2012b. Asthenosphere–lithosphere interaction triggered by a slab window during ridge subduction: trace element and Sr–Nd–Hf–Os isotopic evidence from Late Carboniferous tholeiites in the western Junggar area, NW China. Earth and Planetary Science Letter 329, 84–96.

Tian, R.S., Xie, G.A., Zhang, J., Qu, J.F., Aierkin, A., Li, F.H., Zhang, B.H., Zhao, H., 2017. Deformation characteristics of the Neoproterozoic Langshan Group in Langshan Region and their tectonic implications. Geological Review 5(63):1180 – 1192 (in Chinese with English abstract)

Tian, R.S., Xie, G.A., Zhang, J., Zhu, W.B., Qu, J.F., Gao, S., 2019. Sedimentary provenance and age of the Langshan Group in the northeastern Alxa Block: implications for Neoproterozoic tectonic evolution. Internal

886 Journal of Earth Science 108, 1705–1723.

887 Wang, Q., Xu, J.F., Jian, P., Bao, Z.W., Zhao, Z.H., Li, C.F., Xiong, X.L., Ma, J.L., 2006. Petrogenesis of adakitic
888 porphyries in an extensional tectonic setting, Dexing, South China: implications for the genesis of porphyry
889 copper mineralization. Journal of Petrology 47, 119–144.

890 Wang, B., Cluzel, D., Shu, L., Faure, M., Charvet, J., Chen, Y., Meffre, S., and de Jong, K., 2009. Evolution of
891 calc-alkaline to alkaline magmatism through Carboniferous convergence to Permian transcurrent tectonics,
892 western Chinese Tianshan. International Journal of Earth Sciences, 98, 1275-1298.

893 Wang, B., Jahn, B.M., Lo, C.H., Shu, L.S., Wu, C.Y., Li, K.S., Wang. F., 2011. Structural analysis and 40Ar /39Ar
894 thermochronology of Proterozoic rocks in Sailimu area (NW China): Implication to polyphase tectonics of
895 the North Chinese Tianshan. Journal of Asian Earth Sciences，42(5) : 839–853.

896 Wang, T., Wang, J., Liu, J., 1994. Igneous rock associations and geochemical characteristics of volcanic arc with
897 continental crustal basement in Zongnaishan–Shalazhashan. Geochimica 23, 162–172 (in Chinese with
898 English abstract).

899 Wang, T., Gao, J., Wang, J., Wu, J., 1998. Magmatism of collisional and post–orogenic period in Northern Alaxa
900 region in Inner Mongolia. Acta Geol. Sinica 72, 126–136 (in Chinese with English abstract).

901 Wang, T., Zheng, Y., Gehrels, G., Mu, Z. 2001. Geochronological evidence for existence of South Mongolian
902 micro–continent: a zircon U–Pb age of grantoid gneisses from the Yagan–Onch Hayrhan metamorphic core
903 complex. Chinese Science Bulletin 46, 2005–8 (in Chinese with English abstract).

904 Wang, X.S., Klemd, R., Gao, J., Jiang, T., Li, J.–L., & Xue, S.C., 2018a. Final assembly of the southwestern
905 Central Asian Orogenic Belt as constrained by the evolution of the South Tianshan Orogen: Links with
906 Gondwana and Pangea. Journal of Geophysical Research: Solid Earth, 123, 7361–7388. https://doi.
907 org/10.1029/2018JB015689

908 Wang, Y., Li, J.Y., Sun, G.H., 2008. Postcollisional Eastward Extrusion and Tectonic Exhumation along the
909 Eastern Tianshan Orogen, Central Asia: Constraints from Dextral Strike–Slip Motion and 40Ar/39Ar
910 Geochronological Evidence. The Journal of Geology 116(6):599–618.
911 Wang, Y., Zhou, L.Y., Zhao, L.J., 2013. Cratonic reactivation and orogeny: an example from the northern margin
912 of the North China Craton. Gondwana Res. 24, 1203–1222.
913 Wang, Y., Zeng, Q., Guo, L., and Guo, Y., 2019. Magmatic and tectonic setting of the Permian Au mineralization
914 in the Xing–Meng Orogenic Belt: constraints from the U–Pb ages, Hf–O isotopes and geochemistry of
915 granitic intrusions in the Bilihe and Hadamiao gold deposits: Mineralogy and Petrology, 113, 99–118.
916 Wang, Z.H., Wan, J.L., 2014. Collision–induced Late Permian–Early Triassic transpressional deformation in the
917 Yanshan Tectonic Belt, North China. The Journal of Geology，122(6) : 705 – 716.
918 Wang, Z. Z., Han, B. F., Feng, L. X., Liu, B., 2015. Geochlonology, geochemistry and origins of the Paleozoic–
919 Triassic plutons in the Langshan area, western Inner Mongolia, China. Journal of Asian Earth Sciences, 97,
920 337 – 351. https://doi.org/10.1016/j.jseaes.2014.08.005
921 Winchester, J.A., Floyd, P.A., 1977. Geochemical discrimination of different magma series and their
922 differentiation products using immobile elements. Chem. Geol. 20, 325 – 343.
923 Windley, B.F., Alexeiev, D., Xiao, W., Kröner, A., Badarch, G., 2007. Tectonic models for accretion of the
924 Central Asian Orogenic belt. Journal of Geological Society. London. 164, 31 – 47.
925 Windley, B.F., Xiao, W., 2018. Ridge subduction and slab windows in the Central Asian Orogenic Belt: Tectonic
926 implications for the evolution of an accretionary orogen. Gondwana Research 61, 73–87.
927 https://doi.org/10.1016/j.gr.2018.05.003
928 Wu, T. R., He, G. Q. (1993). Tectonic units and their fundamental characteristics on the northern margin of the
929 Alxa Block. Acta Geologica Sinica (English Edition), 6(4), 373 – 385.

930 Xiao, W.J., Windley, B.F., Allen, M.B., Han, C.M., 2013. Paleozoic multiple accretionary and collisional tectonics
931 of the Chinese Tianshan orogenic collage. Gondwana Research. 23, 1316–1341.
932 Xiao, W.J., Windley, B.F., Sun, S., Li, J.L., Huang, B.C., Han, C.M., Yuan, C., Sun, M., Chen, H.L., 2015. A tale
933 of amalgamation of three collage systems in the Permian– Middle Triassic in Central Asia: oroclines, sutures
934 and terminal accretion. Annual Review of Earth Planetary Science. 43, 477–507.
935 Xiao, W.J., Windley, B.F., Han, C.M., Liu, W., Wan, B., Zhang, J.E., Ao, S.J., Zhang, Z.Y., Song, D.F., 2018,
936 Late Paleozoic to early Triassic multiple roll–back and oroclinal bending of the Mongolia collage in Central
937 Asia: Earth–Science Reviews.186, 94–128.
938 Xie, L., Yin, H.Q., Zhou, H.R., Zhang, W.J., 2014. Permian radiolarians from the Engeerwusu suture zone in Alxa
939 area of Inner Mongolia and its geological significance. Geological Bulletin of China 33 (5), 691–697 (in
940 Chinese with English abstract).
941 Xu, B., Charvet, J., Chen, Y., Zhao, P., Shi, G. Z., 2013. Middle Paleozoic convergent orogenic belts in western
942 Inner Mongolia (China): framework, kinematics, geochronology and implications for tectonic evolution of
943 the Central Asian Orogenic Belt. Gondwana Res. 23:1342–1364.
944 Xu, Z.Q., Li, S.T., Zhang, J.X., Yang, J.S., He, B.Z., Li, H. B., Lin, C.S., Cai, Z.H., 2011a. Paleo–Asian and
945 Tethyan tectonic systems with docking the Tarim block. Acta Petrologica Sinica，27(1) : 1 –22 (in Chinese
946 with English abstract).
947 Xu, Z.Q., Li, H.B., Tang, Z.M., Qi, X.X., Li, H.Q., Cai, Z.H., 2011b. The transformation of the terrain structures
948 of the Tibet Plateau through large–scale strike–slip faults. Acta Petrologica Sinica, 27(11):3157–3170 (in
949 Chinese with English abstract).
950 Yang, T.N., Wang, Y., Li, J.Y., Sun, G.H., 2007. Vertical and horizontal strain partitioning of the Central Tianshan
951 (NW China): evidence from structures and 40Ar/39Ar geochronology. Journal Structural Geology 29,

952 1605 – 1621.

953 Yang, Q.D., Zhang, L., Wang, T., Shi, X.J., Zhang, J.J., Tong, Y., Guo, L., Geng, J.Z., 2014. Geochemistry and
954 LA–ICP–MS zircon U – Pb age of Late Carboniferous Shalazhashan pluton on the northern margin of the
955 Alxa Block, Inner Mongolia and their implications. Geological Bulletin of China 33 (6), 776 – 787 (in
956 Chinese with English abstract).

957 Yin, H. Q., Zhou, H. R., Zhang, W. J., Zheng, X. M., Wang, S. Y., 2016. Late Carboniferous to early Permian
958 sedimentary–tectonic evolution of the north of Alxa, Inner Mongolia, China: Evidence from the Amushan
959 Formation. Geoscience Frontiers 7, 733–741.

960 Yuan, Y., Zong, K., Cawood, P.A., Cheng, H., Yu, Y., Guo, J., Liu, Y., Hu, Z., Zhang, W., Li, M., 2019.
961 Implication of Mesoproterozoic (~1.4 Ga) magmatism within microcontinents along the southern Central
962 Asian Orogenic Belt. Precambrian Research 327, 314–326.

963 Zhang, S.H., Zhao, Y., Song, B., Yang, Z.Y., Hu, J.M., Wu, H., 2007a. Carboniferous granitic plutons from the
964 northern margin of the North China block: implications for a late Palaeozoic active continental margin. J.
965 Geol. Soc. 164, 451 – 463.

966 Zhang, S.H., Zhao, Y., Kröner, A., Liu, X.M., Xie, L.W., Chen, F.K., 2009a. Early Permian plutons from the
967 northern North China Block: constraints on continental arc evolution and convergent margin magmatism
968 related to the Central Asian Orogenic Belt. International Journal of Earth Sciences 98, 1441 – 1467.

969 Zhang, S.H., Zhao, Y., Song, B., Hu, J.M., Liu, S.W., Yang, Y.H., Chen, F.K., Liu, X.M., Liu, J., 2009b.
970 Contrasting Late Carboniferous and Late Permian – Middle Triassic intrusive suites from the northern
971 margin of the North China Craton: Geochronology, Petrogenesis and tectonic implications. Geological
972 Society of America Bulletin 121, 181 – 200.

973 Zhang, J.J., Wang, T., Zhang, Z.C., Tong, Y., Zhang, L., Shi, X.J., Guo, L., Li, S., Zeng, T., 2012. Magma mixing

origin of Yamatu granite in Nuoergong–Langshan area, western part of the Northern Margin of North China Craton: petrological and geochemical evidences. Geol. Rev. 58, 53–66 (in Chinese with English abstract).

Zhang, W., Wu, T.R., Feng, J.C., Zheng, R. G., He, Y.K., 2013a. Time constraints for the closing of the Paleo–Asian Ocean in the Northern Alxa Region: evidence from Wuliji granites. Science China Earth Sciences 56, 153 – 164. http://dx.doi.org/10.1007/s11430–012–4435–y.

Zhang, J.X., Gong, J.H., Yu, S.Y., Li, H.K., Hou, K.J., 2013b. Neoarchean–Paleoproterozoic multiple tectonothermal events in the western Alxa Block, NCC and their geological implication: evidence from zircon U–Pb ages and Hf isotopic composition. Precambrian Research 235, 36–57.

Zhang, J., Li, J., Xiao, W., Wang, Y., Qi, W., 2013c. Kinematics and geochronology of multistage ductile deformation along the eastern Alxa Block, NW China: new constraints on the relationship between the North China Plate and the Alxa Block. Journal of Structural Geology 57, 38–57.

Zhang, X.H., Zhang, H.F., Tang, Y.J., Wilde, S.A., Hu, Z.C., 2008. Geochemistry of Permian bimodal volcanic rocks from central Inner Mongolia, north China: implication for tectonic setting and Phanerozoic continental growth in central Asian orogenic belt. Chemical Geology 249:262 – 281

Zhang, X.R., Zhao, G.C., Eizenhöfer, P.R., Sun, M., Han, Y.G., Hou, W.Z., Liu, D.X., Wang, B., Liu, Q., and Xu, B., 2015a, Paleozoic magmatism and metamorphism in the Central Tianshan block revealed by U–Pb and Lu–Hf isotope studies of detrital zircons from the South Tianshan belt, NW China: Lithos, v. 233, p. 193–208, https://doi.org/10.1016/j.lithos.2015.06.002.

Zhang, J. J., Wang, T., Zhang, L., Tong, Y., Zhang, Z. C., Shi, X. J., et al. 2015b. Tracking deep crust by zircon xenocrysts within igneous rocks from the northern Alxa, China: Constraints on the southern boundary of the central Asian Orogenic Belt. Journal of Asian Earth Sciences, 108, 150 – 169. https://doi.org/10.1016/j.jseaes.2015.04.019

996 Zhang, J., Zhang, Y.P., Xiao, W.X., Wang, Y.N., 2015c. Linking the Alxa Block to the northern margin of the
997 eastern Gondwana during the Early Paleozoic: constraints from detrital zircon U–Pb ages and sandstone
998 composition modes of Cambrian strata. Gondwana Research. 28, 1168–1182.
999 Zhang, X.R., Zhao, G.C., Eizenhöfer, P.R., Sun, M., Han, Y.G., Hou, W.Z., Liu, D.X., Wang, B., Liu, Q., Xu, B.,
1000 and Zhu, Y.L., 2016a, Tectonic transition from late Carboniferous subduction to Early Permian post–
1001 collisional extension in the Eastern Tianshan, NW China: Insights from geochronology and geochemistry of
1002 mafic–intermediate intrusions: Lithos, v. 256–257, p. 269–281,
1003 https://doi.org/10.1016/j .lithos.2016.04.006.
1004 Zhang, J. J., Wang, T., Castro, A., Zhang, L., Shi, X. J., Tong, Y., Maria Iaccheri, L., 2016b. Multiple mixing and
1005 hybridization from magma source to final emplacement in the Permian Yamatu Pluton, the Northern Alxa
1006 Block, China. Journal of Petrology, 57, 933 – 980.
1007 Zhang, X., Zhang, C., Santosh, M., Liu, L., Liu, D., and Luo, Q., 2018a, Early Silurian to Early Carboniferous
1008 ridge subduction in NW Junggar: Evidence from geochronological, geochemical, and Sr–Nd–Hf isotopic
1009 data on alkali granites and adakites: Lithos 300–301,314–329
1010 Zhang, X., Lentz, D.R., Yao, C., Liu, R., Yang, Z., Mei, Y., Fan, X., Huang, F., Qin, Y., Zhang, K., and Zhang, Z.,
1011 2018b. Geochronology, geochemistry, and Sr–Nd–Pb–Hf isotopes of the Zhunsujihua granitoid intrusions
1012 associated with the molybdenum deposit, northern Inner Mongolia, China: implications for petrogenesis and
1013 tectonic setting: International Journal of Earth Sciences, v. 107, p. 687–710.
1014 Zhang, L., Liu, Y.J., Shao, J., Li, W.M., Liang, C.Y., Chang, R.H., Yang, H.Z., Feng, Z.Q., Zhang, C., Xu, J., Shi,
1015 Y., Yang, F., He, P.F., 2019. Early Permian A–type Granites in the Zhangdaqi Area, Inner Mongolia, China
1016 and Their Tectonic Implications. Acta Geologica Sinica (English Edition), 93(5): 1300–1316. DOI:
1017 10.1111/1755–6724.14385

Zheng, R.G., Wu, T.R., Zhang, W., Xu, C., Meng, Q.P., and Zhang, Z.Y., 2014, Late Paleozoic subduction system in the northern margin of the Alxa Block, Altaids: Geochronological and geochemical evidences from ophiolites: Gondwana Research, v. 25, p. 842–858, https:// doi.org/10.1016/j.gr.2013.05.011.

Zheng, R. G., Li, J. Y., Liu, J. F., 2017. The age of volcanic rocks of Amushan Formation on the northern margin of Alxa block: Evidence from zircon U–Pb data. Geology in China 44(3), 612–613 (in Chinese with English abstract).

Zheng, R. G., Zhang, J., Xiao, W, J., 2019a. Association of Permian gabbro and granite in the Langshan, southern Central Asian Orogenic Belt: Age, origin, and tectonic implications. Lithos 348–349, 105174.

Zheng, R.G., Li, J.Y., Zhang, J., Xiao, W.J., Li, Y., 2019b. Early Carboniferous High Ba‑Sr Granitoid in Southern Langshan of Northeastern Alxa: Implications for Accretionary Tectonics along Southern Central Asian Orogenic Belt. Acta Geologica Sinica (English Edition). 93, 820–844.

Zhou, Y. Z., Han, B. F., Xu, Z., Ren, R., Su, L., 2013. The age of the Proterozoic rocks in Yingba area in western Inner Mongolia: constrains on the distribution of the South Gobi micro–continent in the Central Asian Orogenic Belt. Geological Bulletin of China 32 (2–3), 318–326 (in Chinese with English abstract).